EXPLORING DIELS-ALDER REACTIVITY OF ALKYNE-CONTAINING CYCLOPARAPHENYLENES

by

LEYLA GILLETT

A THESIS

Presented to the Department of Chemistry and Biochemistry
and the Robert D. Clark Honors College
in partial fulfillment of the requirements for the degree of
Bachelor of Science

May 2024

An Abstract of the Thesis of

Leyla Gillett for the degree of Bachelor of Science
in the Department of Chemistry and Biochemistry to be taken June 2024

Title: Exploring Diels-Alder Reactivity of Alkyne-Containing Cycloparaphenylenes

Approved: *Ramesh Jasti, Ph.D.*
Primary Thesis Advisor

Many common, commercially available fluorophores exist that have a variety of applications, such as in biological imaging. However, these molecules often have significant limitations, namely photobleaching. As such, continued development of new fluorophores and fluorescent scaffolds is expected to facilitate tasks in areas such as biological analysis, where visualization of systems with consistently good quality and high resolution is vital. Cycloparaphenylenes (CPPs) are of interest in fluorescence research, as these cyclic macromolecules (also referred to as "nanohoops") are promising candidates for fluorescent scaffolds, because not only do they generally overcome these limitations, but they also have tunable fluorescence based on their size and functionality.

While synthetic routes for achieving [n]cycloparaphenylenes ([n]CPPs, where "n" refers to the number of ring units within the larger nanohoop) have been well-established, further exploration of certain types of these fluorescent molecules continue to show interesting results, including as alternative fluorophores for live cell imaging. This research examines the [9+1] internal alkyne-containing CPP (which contains 9 phenyl units, plus an integrated carbon-carbon triple-bond unit, hence the "9+1"), where the distortion of the alkyne unit promotes increased reactivity that will allow for the synthesis of a range of undiscovered CPP derivatives. This project highlights new routes for synthetic exploration with these uniquely fluorescent nanohoops, motivated by utilizing angular-strained motifs and classic Diels-Alder reactions. As molecular properties generally change with different functionalities, the reactivity and photophysical properties of the class CPP derivatives explored here are unprecedented.

After completing the synthesis of the [9+1]CPP following an established synthetic route, Diels-Alder reactivity was explored with tetraphenyl cyclopentadienone (TPCPD) in order to

introduce new functionality at the site of the alkyne. TPCPD was selected as it is an important building block for many organic and organometallic compounds, and there are literature precedents describing the potential of the central ring to react as a diene with dienophiles in a Diels-Alder reaction, similar to the alkyne in the [9+1]CPP. This successful late-stage functionalization of a fluorophore in relatively high yield (69%) shows promising results as a new way to achieve desired modifications of fully-synthesized CPPs, opening new avenues for research into molecules capable of "clicking" to the alkyne-containing CPP that provide useful functions.

Acknowledgements

This project was funded in part by the Thomas and Lindsey Marriott Undergraduate Research Support Fund, which has generously aided me in allowing me to focus on my research while being a full-time student.

I would like to thank Dr. Ramesh Jasti for giving me the incredible opportunity to be a part of his research group, which has been the highlight of my undergraduate career and has inspired me to continue my studies as a graduate student. I would also like to extend this gratitude to all of the Jasti Lab members, who have provided a welcome, encouraging, and positive environment inside and outside of the lab space. Their dedication, knowledge, and problem-solving skills continue to inspire me in my endeavors.

I would also like to thank Dr. Lindsay Hinkle, for her assistance throughout this project and for her advice and insights during our conversations both inside and outside of the classroom. Her dedication to teaching and improving science communication and understanding continues to motivate me to be a better scientist and communicator.

I would especially like to thank Tara Clayton, my graduate student mentor, for helping me grow as a scientist and person in the last two years. She has provided me with invaluable guidance, motivation, support, and has been an excellent mentor and role model. Without her assistance, this project would have not been possible. I truly appreciate her taking me on as an undergraduate mentee, and she has inspired me to seek opportunities to be a mentor as a graduate student myself in the future.

Finally, I would like to thank all my family and friends who have supported me throughout my undergraduate career. They have made navigating this journey so much easier, and I could not have accomplished everything without their unwavering support.

Table of Contents

List of Figures

Chapter I. Background

I.I Introduction to Fluorescence

Fluorescence is a property of some molecules that, after absorbing radiation, emit visible light. Fluorescent molecules have demonstrated useful applications in areas such as biological imaging[1]. This process is initiated when a photon of a certain energy interacts with an electron of the molecule in its ground state, increasing the electron's energy to an excited state. The electron's energy depletes as it relaxes to the lowest excited state, and eventually decays to the ground state through the emission of a photon of light[2]. This emitted photon is the basis of a molecule's fluorescence, which ultimately contains information about the molecule itself. A visualization of this cyclical process is shown in Figure 1.

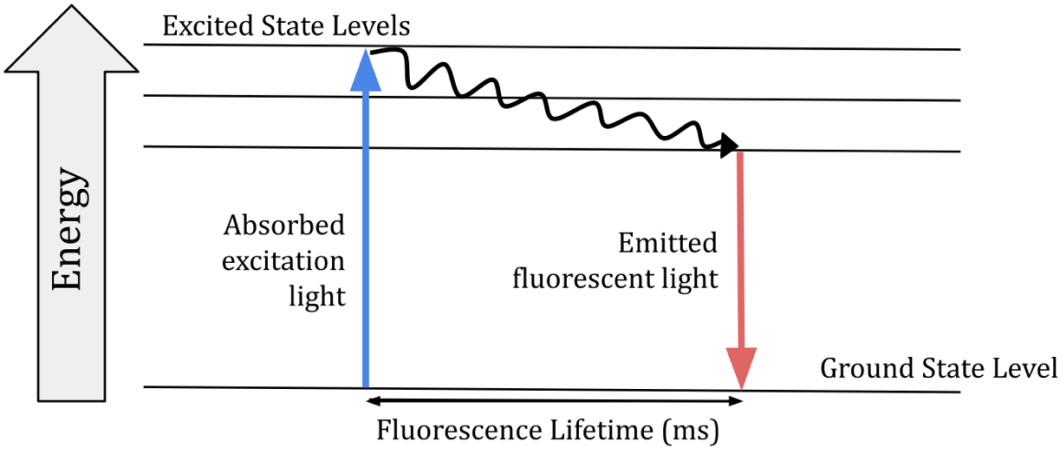

Figure 1. The overall absorption and emission process that produces fluorescence in a fluorophore.

In order to decode the information contained in a molecule's fluorescence, the brightness of the fluorophore must first be characterized. This is typically done in accordance with its quantum yield and extinction coefficient, which are a representation of the number of emitted photons relative to the number of photons used in the initial excitation, and a measure of how

well the fluorophore absorbs a certain wavelength of light, respectively. Together, these two values represent how well a fluorescent molecule absorbs, then re-emits light.

Within any atom, there are orbitals of different energy levels that may or may not contain electrons. When the molecule, which is made up of different atoms, is at its ground state (i.e. lowest energy level), orbitals that correspond to higher energy levels are generally unoccupied, whereas the opposite is true when the molecule is in an excited state (i.e. higher energy level). Interactions between these atomic orbitals to form bonds within the molecule result in a series of molecular orbitals that comprise the molecule itself—its electronic structure. The occupation of these orbitals by electrons is systematic in nature, and interactions between the molecular orbitals form the basis of fluorescence. When an electron is excited (i.e. receives energy, in the form of light), it will jump from a lower-energy orbital to a higher-energy orbital, the latter of which is usually unoccupied due to an energetic barrier. When the electron eventually returns to its "normal" ground-state energy level, the difference in energy between both levels determines the energy (and thus wavelength/color) of the photon that is emitted by the fluorophore. This is usually represented as the energy difference between the highest-occupied and lowest-unoccupied molecular orbitals (generally referred to as HOMO and LUMO, respectively), although it is generally understood that these electronic transitions may occur from other orbitals. A general representation of the trend in the color of an emitted photon and the associated difference in HOMO- and LUMO- energies (generally referred to the HOMO-LUMO gap, or bandgap) is shown in Figure 2. As the bandgap energy decreases, the fluorophore emission is more red-shifted, whereas as the bandgap energy increases, it is more blue-shifted. Thus, information about the structure of the molecule is contained in the characteristics of the fluorophore emission[3].

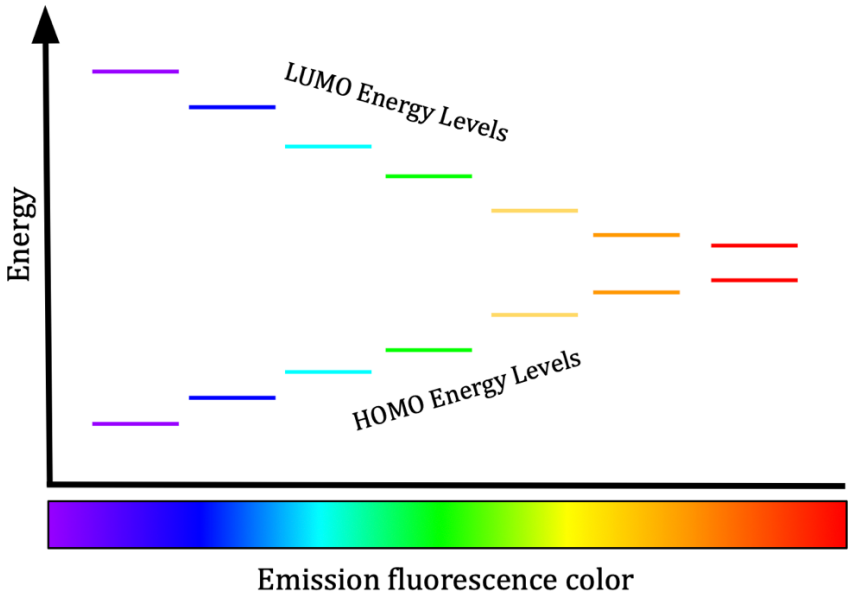

Figure 2. Visualization of HOMO-LUMO gaps and corresponding fluorescent emission colors.

I.II Common Fluorescent Scaffolds and CPPs

Many common fluorophores exist that have a variety of applications, such as in biological imaging[1]. The majority of commercially available fluorophores are based on four fluorescent scaffolds: cyanine, fluorescein, bodipy, and coumarin. Structures of these fluorophores are shown in Figure 3. Since these fluorophores still have significant limitations that cause loss of fluorescence (temporarily, in certain conditions, or permanently), the exploration of new potential fluorescent scaffolds should prove extremely valuable. Fluorescein (Figure 3a), for example, is typically used as a contrast agent in medical imaging. However, it can undergo a structural change at biological pH that causes a loss of fluorescence[4]. Additionally, fluorophores such as cyanine (Figure 3b) and fluorescein (Figure 3a) dyes, which are also used in fluorescence imaging of biological structures, that are exposed repeatedly or for long amounts of time to an excitation light source may also undergo structural changes to non-fluorescent conformations through a process called photobleaching[5]. Continued development of new fluorophores and fluorescent scaffolds is expected to facilitate tasks in areas such as

biological analysis, where visualizing systems of interest is important. The class of macromolecules known as cycloparaphenylenes (CPPs) have become a definite area of interest in fluorescence research, as their extinction coefficients and quantum yields are generally high, meaning they tend to fluoresce brightly and for a longer time.

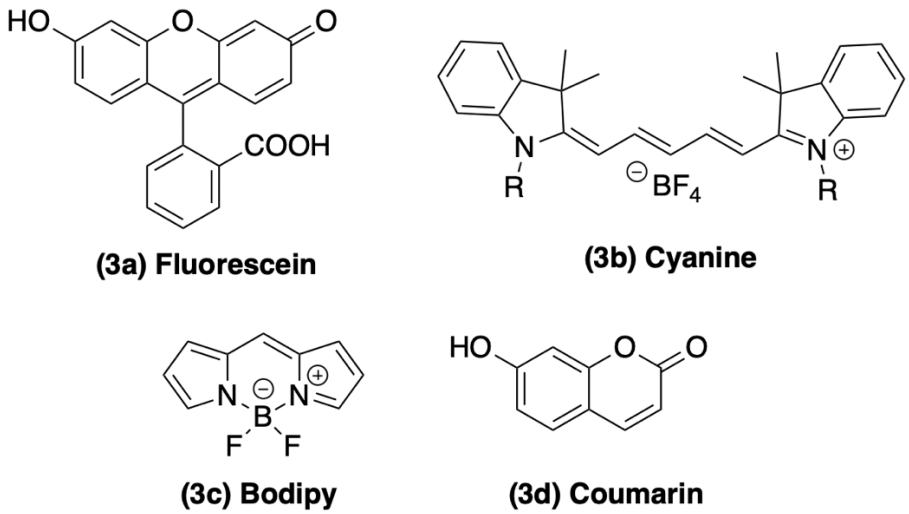

Figure 3. Structures of common fluorescent dyes: (a) Fluorescein, (b) Cyanine, (c) Bodipy, (d) Coumarin.

These cyclic macromolecules, also referred to as “nanohoops”, are very promising candidates for fluorescent scaffolds because they also have tunable fluorescence based on hoop size and functionality. The core structure of a CPP contains a series of benzene rings, cyclically linked in the *para*-positions, and essentially represents the smallest cross section of a carbon nanotube (CNT). An example CPP, CNT, and the different types of connectivity are shown in Figure 4.

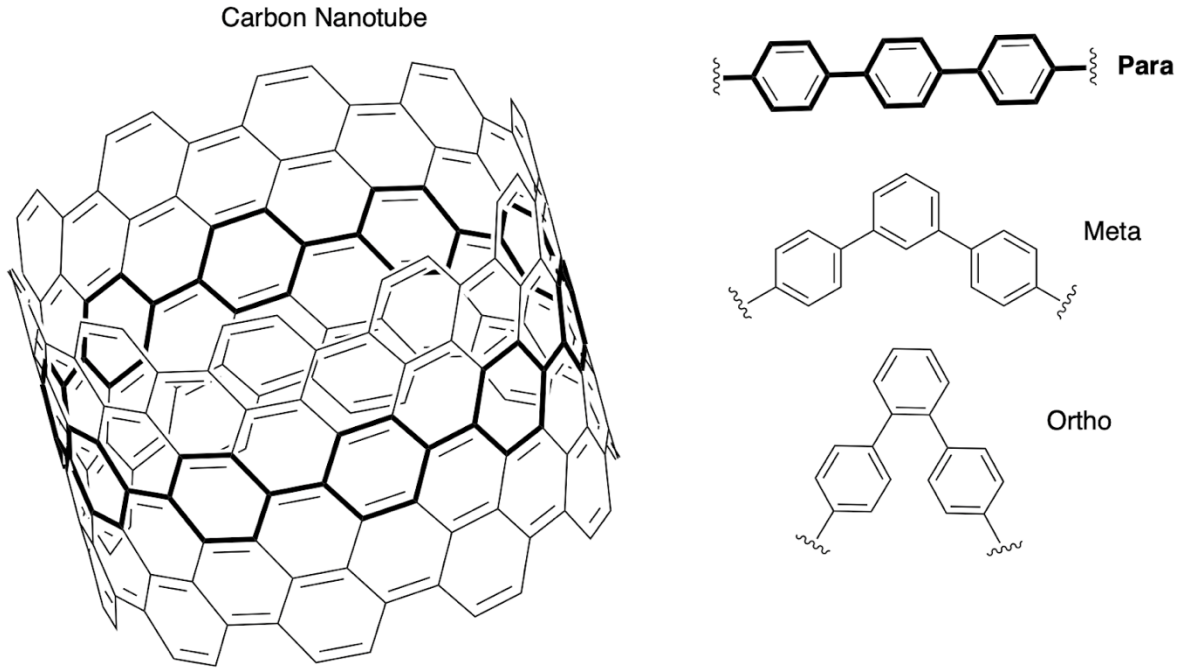

Figure 4. Example CNT, with the smallest cross section in bold. Possible connectivity of the aromatic units is shown (ortho, meta, para).

Cycloparaphenylenes composed of "*n*" benzene rings are generally referred to as [*n*]CPPs, and the highly-strained, radially-oriented **π**-system (involving orbitals associated with the bonds in each benzene ring, shown in Figure 5) leads to unique reactivities[6-7]. This conjugation results in optoelectronic properties that are size-dependent[6-10], including fluorescence. The radially-oriented **π**-system and a visualization of the size-dependent fluorescence of different CPPs are shown in Figure 5 and 6, respectively.

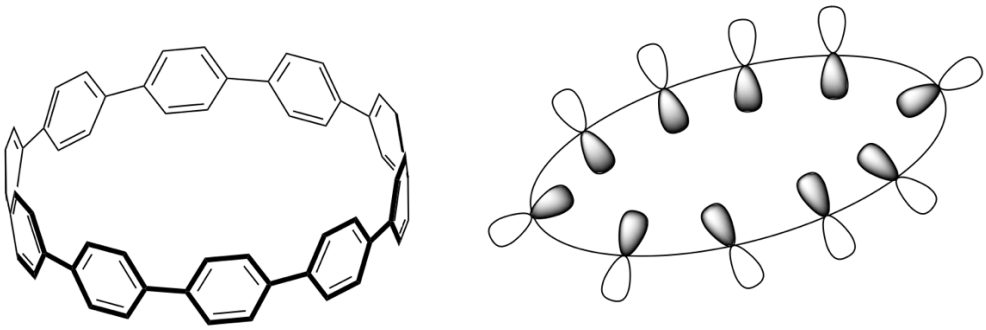

Figure 5. Typical CPP structure (left), and a simplified representation of the radially-oriented **π**-orbital system (right).

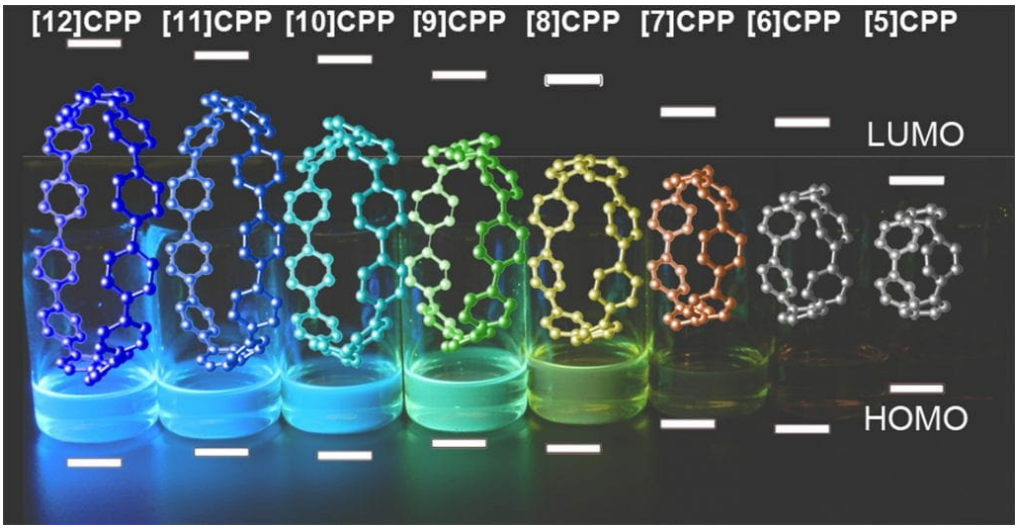

Figure 6. Different sizes of CPPs with their respective fluorescence, including a visual representation of the HOMO-LUMO gaps[11].

CNTs, like CPPs, are carbon-based nanomaterials. CNTs have many desirable potential applications, including enabling faster and stronger electronic devices, improved sensors for disease detection, more efficient energy generation and storage, among others[12]. Achieving synthesis of CPPs was originally with the goal of using them as building blocks for successful, controlled synthesis of CNTs, as synthetic methods for CNTs generally resulted in a mixture of undesired sizes and lengths[7]. The synthesis of CPPs was first accomplished via a stepwise method which has since allowed for significant structural customization[13-15] (i.e. size, functionality). Modifications of the basic CPP scaffold structure may have unprecedented utility

and applications, potentially improving on some of the aforementioned limitations of other common fluorophores. Consequently, current CPP research has focused on introducing new types of functionalities to design synthetic polymers, rotaxanes, biological probes, and many others[16-19].

I.III Alkyne-Containing CPPs

Introduction

Although the first recorded attempted synthesis of cycloparaphenylene-like structures was in 1934[20], only in 2008 were the first syntheses of [9], [12], and [18]CPPs successful[6-7]. Since this initial success, continued refinement and development has allowed for the synthesis of many different CPP sizes, some of which were discussed earlier in this article (Figure 6) in terms of their tunable, size-dependent fluorescent capabilities. Synthesis of alkyne-containing CPPs is of significant interest due to the unique structural components, and subsequent reactivities, that may provide avenues for further synthesis of novel CPP derivatives through selective, late-stage functionalization.

Alkyne-containing CPPs are a class of macrocyclic angle-strained alkynes achieved through a combination of different synthetic building blocks[21]. Typically, alkynes (i.e. triply-bonded carbons) prefer a linear structure due to the rigid overlap of the orbitals involved in the two **π**-bonds. Angle-strained cycloalkynes are arbitrarily defined[22] as cyclic molecules involving a triple-bond where the C–C–C bond is deformed by at least 10°, and have been of interest to researchers due to the unique reactivity associated with this distortion[21]. The incorporation of an alkyne unit into the backbone of the CPP introduces angular strain into the alkyne, ultimately increasing reactivity at that site. In Figure 7, there is more strain (red) on the side of the ring opposite of the alkyne as the system attempts to mitigate (i.e. redistribute) the strain on the

alkyne itself. There is further evidence of this trend, in that adding meta-linkers directly opposed to the alkyne further increases the molecular strain[23].

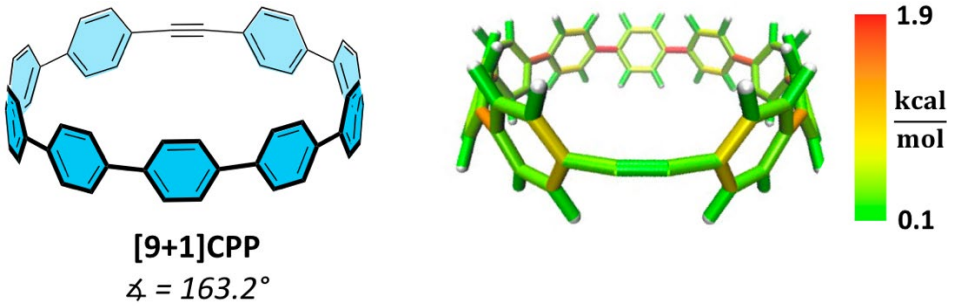

Figure 7. StrainViz calculation for [9+1] CPP, showing the strain distribution in the CPP system with an integrated the alkyne unit[23].

Cycloparaphenylenes containing an alkyne within the backbone afford a promising method of combining a uniquely fluorescent scaffold with desired functionality in a concise, selective way[1,21]. Alkyne-containing CPPs of various sizes can undergo cycloadditions at the site of the alkyne without a catalyst and at temperatures as cold as 0°C, whereas comparable reagents capable of strain-promoted cycloadditions (e.g. dibenzo-fused cyclooctyne and its derivatives) often require at least heating in order for such a reaction to occur[21]. By achieving milder conditions, this reaction opens new doors for synthetic exploration, and functionalization of these molecules as novel fluorophores that overcome typical fluorophore limitations. In other words, not only does this CPP constitute a reliable, consistently-fluorescent molecule, but also it can be combined with other molecules to achieve a specific function (e.g. targeted drug delivery and monitoring). Discovering accessible, efficient, and reliable ways to explore new molecular properties resulting from joining smaller molecular building blocks is the fundamental logic associated with these 'click' reactions[22]. As such, the synthesis of angle-strained alkynes and exploration of their unique reactivities continues to be of interest, including alkyne-containing macrocyclic structures such as the [9+1] CPP.

Synthesis

Angle-strained cycloalkynes are synthetically challenging, as the distortion of the alkyne unit leads to instability, due to the increased reactivity[21]. Previous attempts at the synthesis of smaller cycloalkynes[24,25] were observed to have short lifetimes as a result of this instability. Larger cycloalkynes afford more stability (i.e. less angle strain), and thus longer molecular lifetimes, allowing them to be potentially isolated. The smallest isolated cycloalkyne (cyclooctyne) and the core structures of other smaller, transient intermediate examples are shown in Figure 8[26].

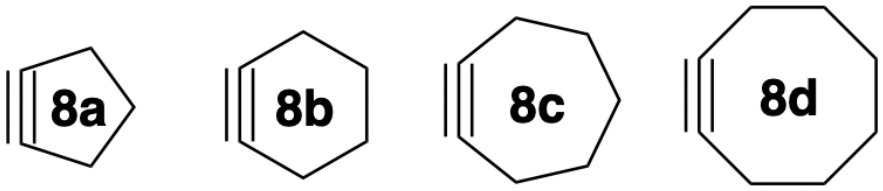

Figure 8. Cyclo- (a) -pentyne, (b) -hexyne, (c) -heptyne, and (d) -octyne chemical structures. As the ring size increases, the amount of angle-strain on the alkyne unit decreases.

Alkyne-containing CPPs were first achieved through a stepwise synthesis in 2018, affording various sizes, of which the [11+1] internal alkyne CPP was the largest[21]. The [11+1] CPP system is of interest for this reason, but the reactivity at the alkyne site in the [11+1] CPP has been explored in a variety of ways, including with a Diels-Alder reaction. This project instead involves the use of the [9+1] CPP, which due to its smaller size (and thus larger amount of strain) was hypothesized to show increased reactivity (i.e. achieving product in comparably high yield under more mild reaction conditions). The outlined synthetic method is shown in Figure 9, including the final Diels-Alder reaction.

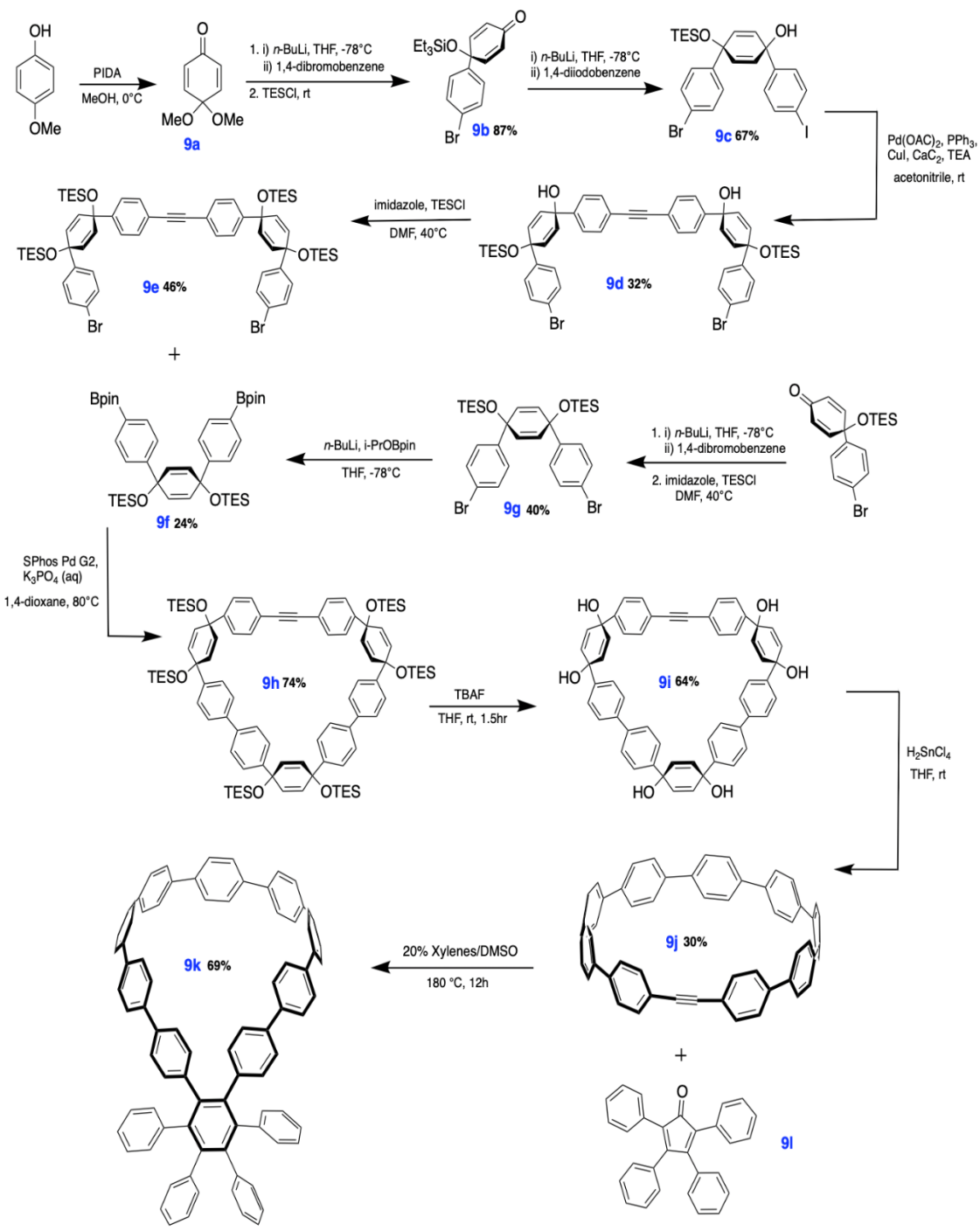

Figure 9. Synthesis of [9+1] CPP and Diels-Alder reaction with TPCPD.

Beginning with the oxidative addition of methanol to commercially available 4-methoxyphenol, **9a** is then combined with commercially available 1,4-dibromobenzene via lithiation-addition in two steps (i.e. lithium-halogen exchange, then nucleophilic addition, see

Materials and Methods section). **9b** is then TES-protected, which not only prevents unwanted side reactions at the site of the alcohol (OH) group, but also favors the cis-geometry, which is a necessary structural feature in the final coupling partner (see Materials and Methods section). TES-protected **9b** is then subjected to another round of lithiation-addition, with commercially available 1,4-diiodobenzene. **9c** is then coupled with another equivalent of itself through a double-Sonogashira reaction, and the carbon-carbon triple bond is installed with the help of various metal catalysts (see Materials and Methods section). **9d** is then TES-protected for similar reasons, and **9e** is combined with **9f** in a Suzuki cross-coupling reaction (see Materials and Methods section). **9f**'s synthetic precursor, **9g**, was synthesized in a similar manner to **9c**, but involves combining **9b** and 1,4-dibromobenzene instead. **9g** is then borylated, installing boronic ester ("Bpin") groups through a lithium-halogen exchange, then addition of an electrophilic source of boronic ester. Following the Suzuki coupling of **9e** and **9f** (to yield **9h**), the TES-protected hydroxyl groups are deprotected (**9i**), and the macrocycle is subjected to aromatization conditions (**9j**), which ultimately reforms the aromatic benzene units in the original component molecular building blocks. To perform the Diels-Alder reaction, **9j** was combined with **9l** in a manner described in the next section, to yield the final product **9k**.

I.IV Diels Alder Reactions

Introduction to Click Chemistry

Synthetic organic chemistry is at its core an imitation of fundamental, naturally occurring processes. As new discoveries are made and developments occur, synthetic methods are continuously improved in order to, ultimately, afford new molecules with desired properties. Click chemistry has grown in popularity among chemists since the term was introduced in 2001[24] to describe the high efficiency and reproducibility associated with these types of

reactions[22,24,25,27]. Click reactions have a reputation as reliable and stable, often utilizing functionalized molecules that possess an increased reactivity, such as the site of the angle-strained alkyne in the [9+1] CPP. There are many types of click reactions, of which a few commonly used ones are depicted in Figure 10. Some require a catalyst such as copper (Figure 10b), others rely on stain-promoted reactivities (Figure 10a), and some will occur under favorable thermodynamic conditions (i.e. Diels-Alder, Figure 11).

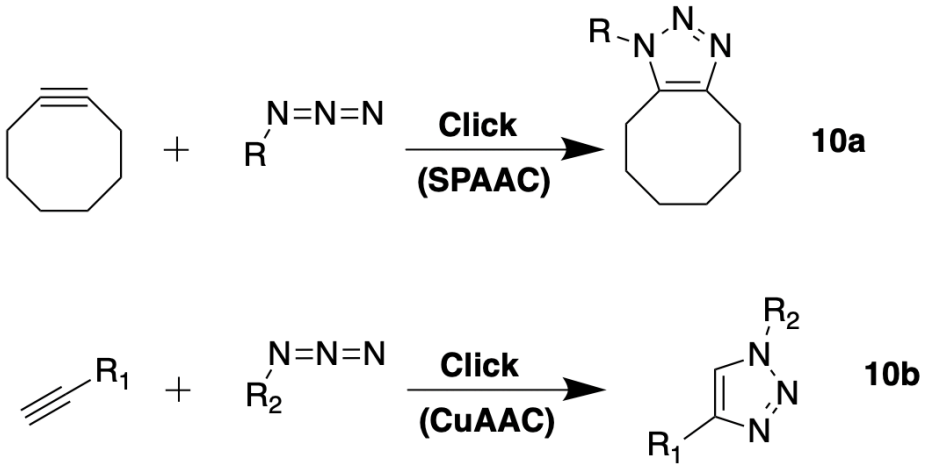

Figure 10. Other common examples of Click chemistry: (a) strain-promoted azide-alkyne cycloaddition (SPAAC), (b) copper-catalyzed azide-alkyne cycloaddition (CuAAC).

The Diels-Alder reaction, first discovered by Otto Diels and Kurt Alder in 1928[28], involves the reaction of two molecules to form two new C–C bonds. Notably, these new bonds are ***σ***-bonds, which are more stable in energy than the **π**-bonds initially involved in the formation of the new bond[28]. An example Diels Alder reaction is depicted in Figure 11, where 1,3-butadiene and ethylene are reacted to form cyclohexene. The four **π**-electrons in the conjugated diene (1,3-butadiene) and two **π**-electrons in the dienophile (ethylene) shift to form the two new C–C bonds in the product via a cyclic transition state, hence the term "[4+2] cycloaddition".

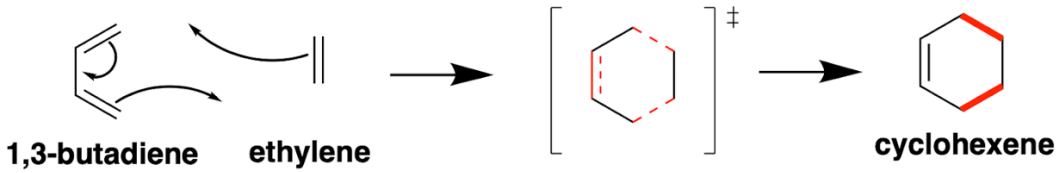

Figure 11. Diels-Alder reaction mechanism for 1,3-butadiene and ethylene to form cyclohexene.

Diels-Alder reactivity has many potential uses as a clickable chemical reaction, such as in pharmaceutics and bioengineering[29-31], among others. Since Diels-Alder cycloadditions do not require metal catalysts, which are often toxic, they have emerged to the forefront as one of the most useful reactions in synthetic organic chemistry[29]. Instead, Diels-Alder reactions proceed under mild conditions, forming products in high yields, while minimizing harmful byproducts[30]. Combined with a reactive CPP scaffold, we postulate that the synthesis of many new uniquely fluorescent derivatives with unprecedented properties via a Diels-Alder reaction will be possible.

TPCPD Reactivity

Tetraphenyl cyclopentadienone (TPCPD) is an important building block for many organic and organometallic compounds[32]. Previous studies have indicated that TPCPD and other cyclopentadienone derivatives are capable of Diels-Alder reactivity with a variety of substituted alkynes, achieving cycloaddition under mild conditions with high yield[33-34]. In TPCPD (Figure 12), the central ring reacts as a diene with dienophiles[33] to achieve the Diels-Alder product in high yield.

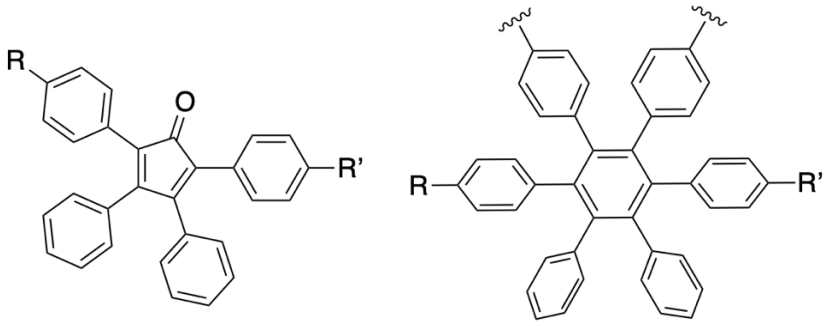

Figure 12. Chemical structure of (left) tetraphenyl cyclopentadienone (R, R' = H), and (right) the hexaphenyl benzene moiety that results from a Diels-Alder reaction of the central dienone ring.

As discussed in the previous section, the formation of two new, stable C–C $\boldsymbol{\sigma}$-bonds under mild reaction conditions is what makes this reaction unique. Paired with a reactive alkyne dienophile, such as the angle-strained cycloalkyne in the [9+1] internal alkyne CPP, the reaction is expected to proceed with moderate-to-high yield, affording the Diels-Alder product (see next chapter, Figure 13), ultimately introducing new functionality at the site of the alkyne.

Chapter II. The Diels-Alder Product

II.I Characterization

Standard characterization methods provide strong evidence of the formation of the expected product of the Diels-Alder reaction (Figure 14) between tetraphenyl cyclopentadienone and the [9+1] internal alkyne CPP. Manual integration of the ^{1}H NMR spectrum in deuterated chloroform (Figure 13) yields a total of 56 protons, which aligns with the expected total of 56 hydrogens based on the structure drawn in Figure 14. Presently, ^{13}C NMR has not yet been performed due to time constraints, however it is expected that the ^{13}C NMR spectrum will provide further evidence in favor of the formation of this product.

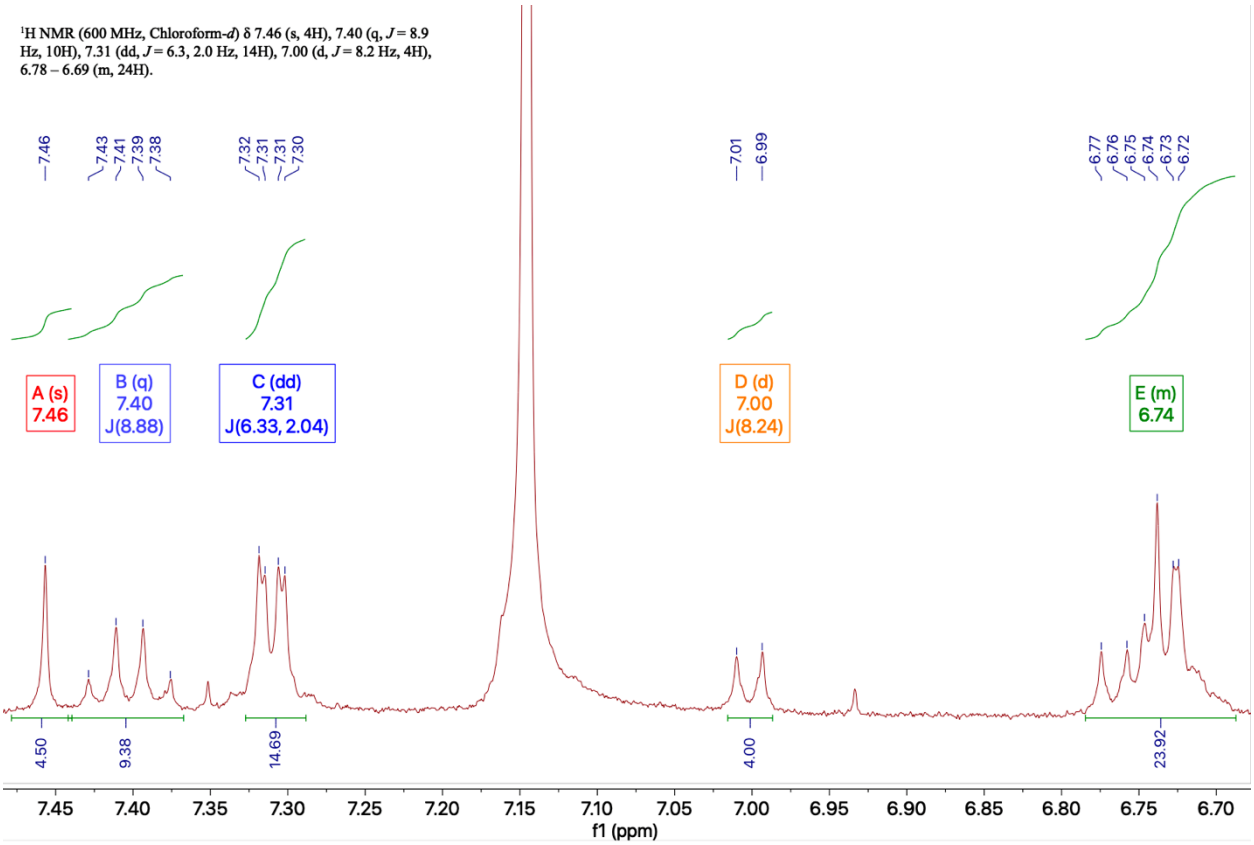

Figure 13. ^{1}H NMR characterization of the TPCPD and [9+1] CPP Diels-Alder product.

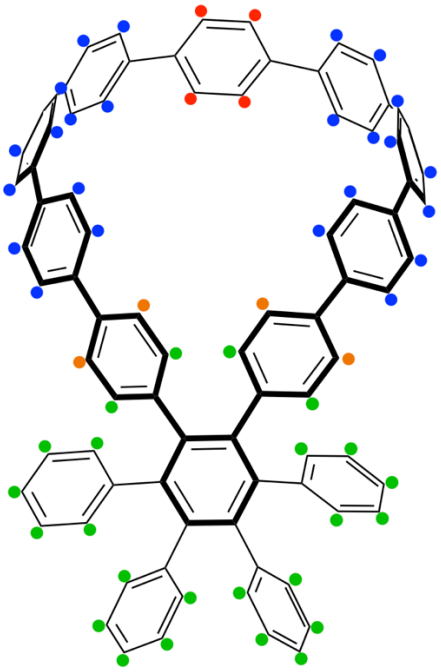

Figure 14. Molecular structure of the TPCPD and [9+1] Diels-Alder product, including proposed ^{1}H NMR signal assignments (see colors and Figure 13).

In order to quantify the fluorescence, standard fluorimetry and UV-vis were performed on the sample, dissolved in dichloromethane. The normalized intensities as a function of wavelength are shown in Figure 15, where the peak absorbance and fluorescence wavelengths are 327 nm and 473 nm, respectively.

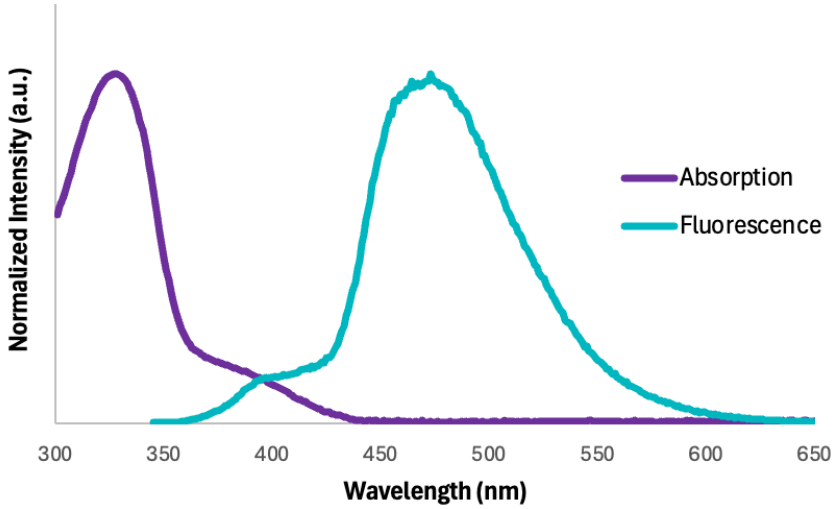

Figure 15. Normalized absorbance and fluorescence data for the Diels-Alder product.

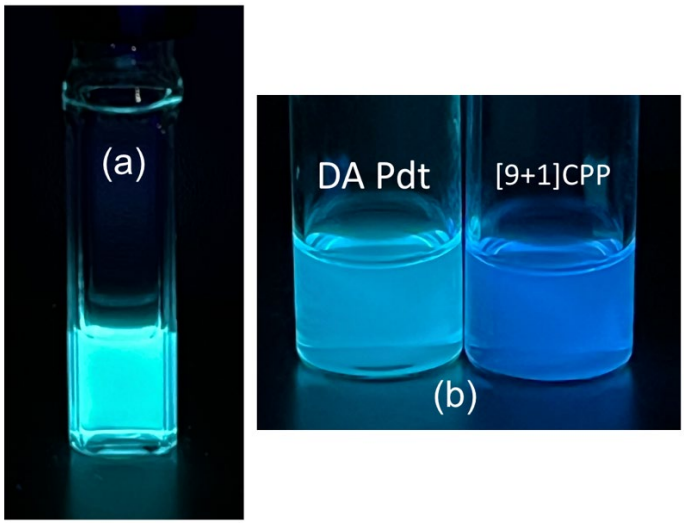

Figure 16. Visible fluorescence in DCM of (a) the Diels-Alder product under UV light, and (b) a side-by-side comparison with [9+1] CPP.

II.II Conclusions and Future Directions

As evidenced in earlier discussions, utilizing the classic Diels-Alder reaction as a means for late-stage functionalization of these fluorophores shows promise for a wide variety of unprecedented applications. The absorbance/fluorescence profile is consistent with those of comparable CPPs[7], which indicates a retention of the fluorescence properties that make CPPs special. For comparison, the maximum wavelengths of absorbance and emission, for the standard

[9+1]CPP, are 342 nm and 463 nm, respectively[21]. We expect that the slight red-shift in the maximum emission wavelength (and associated color, which is more green-teal than blue) is due to the increased conjugation in the Diels-Alder product compared to the parent [9+1]CPP. While further exploration is required, this initial success paves the way for possible experimentation with other dienes, such as TPCPD derivatives or other molecules capable of Diels-Alder reactivity, or even other types of alkyne-containing CPPs (e.g. [7+1]CPP, which may require even milder conditions to achieve desired product conversion due to the increased strain resulting from the smaller ring size). By developing this synthetic route to reliably and reproducibly 'click' a dienophile selectively to the CPP's alkyne site, while maintaining key physical properties of the CPP backbone, this project ultimately unlocks new molecular design possibilities in fluorescence research.

Chapter III. Materials and Methods

III.I Overview

Synthesis of the cycloparaphenylene begins using commercially available reagents to create small, curved building blocks (coupling partners). These pieces are then assembled, functionalized, and linked together to create a larger cyclic structure (macrocycle) of desired size, and eventually the corresponding cycloparaphenylene (CPP). Purification of these intermediates, to isolate them from unreacted starting material and unwanted byproducts, was done with a variety of techniques that included: filtration, liquid-liquid extraction, vacuum distillation, thin-layer chromatography (TLC), and flash column chromatography. Characterization with ^{1}H NMR techniques after each step of the synthesis, when possible, allowed for confirmation that the desired reaction did occur, and the desired products were formed.

III.II Reaction Procedures

Unless otherwise specified, all of the following reactions were performed in flame-dried glassware (which was dried under vacuum) and under an inert nitrogen atmosphere to avoid the accumulation of water and air that could disrupt the reaction. Solid state reagents were dried under vacuum (or flame-dried when possible) prior to use, and liquid state reagents were transferred to the reaction vessel using needles and syringes (from storage under an inert atmosphere) in order to further minimize air and water exposure.

Lithiation Addition

This reaction is an important step in the synthesis of CPPs as it forms a new carbon-carbon bond that connects two rings together. It involves a lithium-halogen exchange, followed

by nucleophilic addition to a ketone, for which a typical scheme is shown in Figure 17. An alkyl-lithium reagent (e.g. ***n*-butyllithium**) is combined with an aryl halide (e.g. **1,4-dibromobenzene**) in a tetrahydrofuran (THF) solution at -78 °C. The ketone substrate is then slowly added, and the reaction is allowed to stir for an hour. Then, in this case, *in-situ* TES-protection is performed, and the reaction mixture is allowed to warm to room temperature. Lithiation-addition reactions are typically quenched with deionized water.

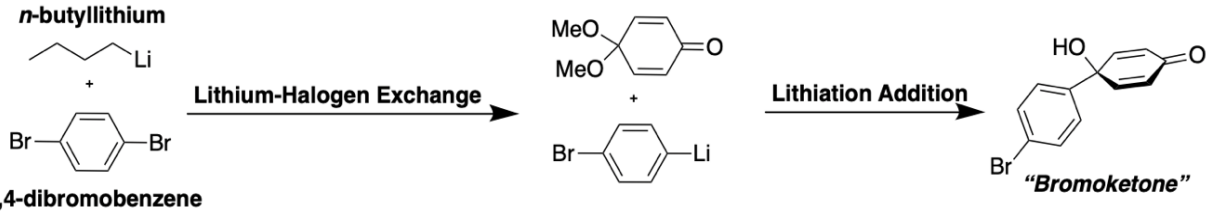

Figure 17. Reaction scheme for lithiation additions, including the lithium-halogen exchange step.

TES Protection

Triethyl silyl (TES) protection of the hydroxy (OH) group hydrogens within a molecule allows for stereoselectivity in further additions (i.e. a more favorable cis-addition). The bulky TES groups sterically hinder one face of the molecule, effectively promoting reactivity at the desired site. This reaction, for which scheme is shown in Figure 18, involves combining a molecule containing hydroxy groups (e.g. ***bromoketone***) and imidazole in a dimethylformamide (DMF) solution. Chlorotriethylsilane (TESCl) is then added dropwise, and the reaction mixture is allowed to stir overnight at 40 °C. TES-protection reactions are typically quenched with aqueous sodium bicarbonate.

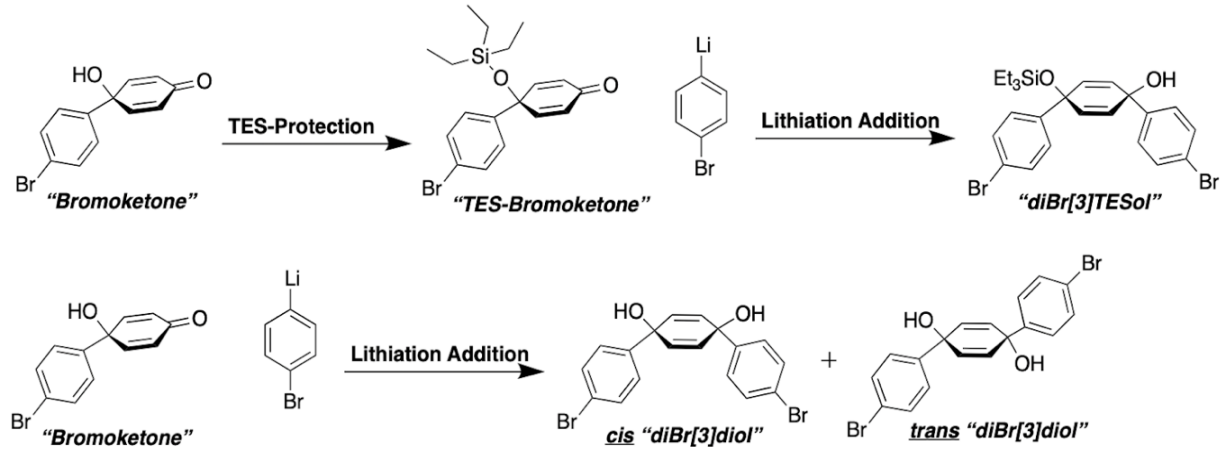

Figure 18. Overall reaction scheme for TES-protections. Also shown is the impact of the additional TES group on the stereoselectivity of a lithiation addition reaction, which heavily favors the cis-product.

Miyaura Borylation

Similar to lithiation-addition reactions, the mechanism of lithiation-borylation begins with a lithium-halogen exchange. The general reaction scheme is shown in Figure 19, which first involves combining a halide-containing molecule (e.g. ***diBr[3]diTES***) and an alkyl-lithium reagent (e.g. ***n*-butyllithium**) in a THF solution at -78 °C. Then, an electrophilic source of boronic ester reagent is added (e.g. ***i-PrOBpin*** or $\boldsymbol{B_2pin_2}$) and the reaction mixture is allowed to warm to room temperature overnight while stirring before being quenched with deionized water. Miyaura borylation reactions allow for the installation of ***Bpin*** groups, which are an important precursor for the future Suzuki cross-coupling reaction.

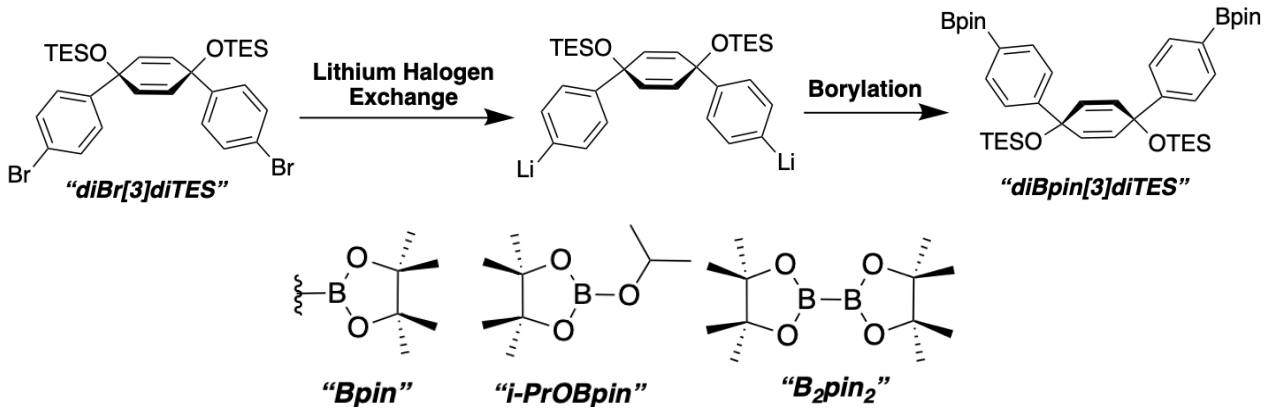

Figure 19. Miyaura borylation reaction scheme, including structures for relevant abbreviations.

Sonogashira Reaction

The palladium-catalyzed Sonogashira reaction involves the formation of a new carbon-carbon bond between a terminal alkyne and a halide-containing molecule (e.g. ***bromoiodo[3]TESol***). A double-Sonogashira reaction repeats this process twice, for a total of two new carbon-carbon bonds on either side of the alkyne, as shown in Figure 20. This reaction involves combining the palladium catalyst (i.e. palladium acetate), triphenylphosphine, and copper iodide in a wet (water-containing) acetonitrile solution that is then sparged with nitrogen gas. The alkyne source (e.g. calcium carbide) and base (e.g. triethylamine) are then added to the reaction mixture, and the solution is allowed to stir at room temperature under an inert atmosphere for 24 hours.

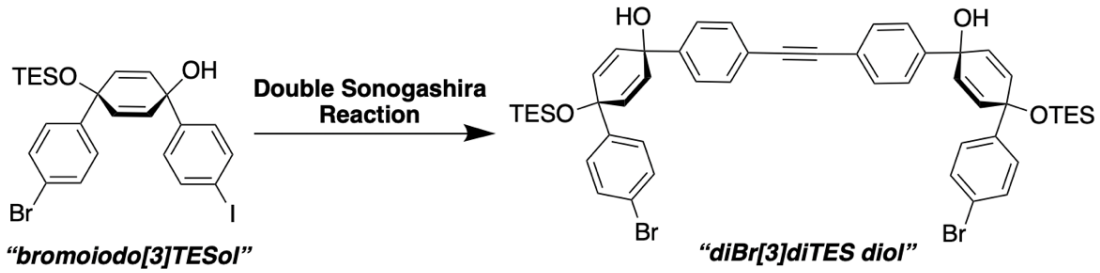

Figure 20. Double-Sonogashira reaction scheme. In this case, the integration of the alkyne unit is also performed in this step, yielding the symmetrical Double-Sonogashira product that includes the alkyne.

Suzuki Macrocyclization

Similar to the Sonogashira reaction, Suzuki cross-coupling reactions also involve the use of a metal catalyst to create new carbon-carbon bonds between two molecules (highlighted in Figure 21). This step is crucial, as it forms the macrocycle (e.g. ***[9+1]mac hexaTES***) which in the next steps will become the CPP, and it is performed on a very small scale in order to favor intramolecular Suzuki coupling, rather than intermolecular coupling. These distinctions are illustrated in Figure 17. This reaction involves the combining both coupling partners (e.g. ***diBr[6+1]tetraTES*** and ***diBpin[3]diTES***) with the palladium catalyst (i.e. SPhos Pd G2 or G3) in a 1,4-dioxane solution. The reaction mixture is then sparged with nitrogen gas at room temperature, then heated to 80 °C. An aqueous tripotassium phosphate solution is then slowly added, and the reaction mixture is allowed to stir overnight under an inert atmosphere, and then is removed from heat and allowed to cool to room temperature.

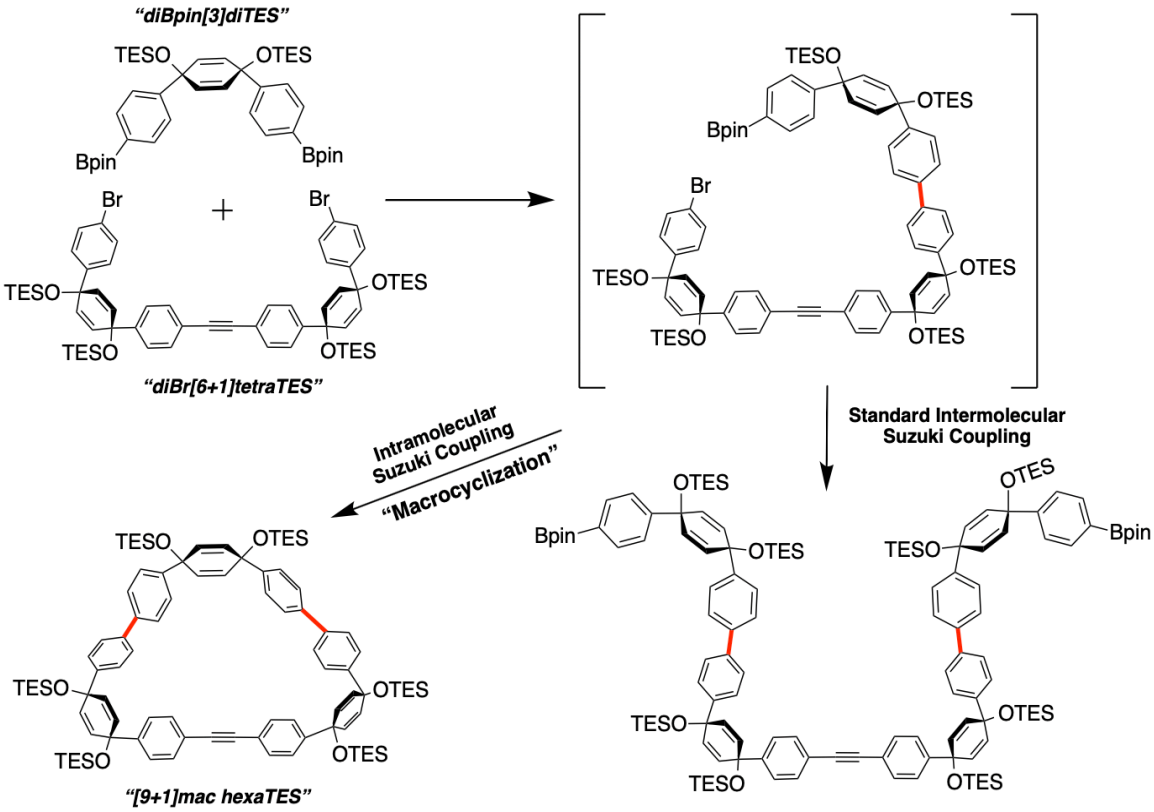

Figure 21. Possible products of this Suzuki coupling reaction, including the desired macrocyclic product. Newly-formed bonds are shown in red. With dilute reaction conditions, intramolecular coupling is favored.

Deprotection and Aromatization

Deprotecting (i.e. reverting the previously-installed TES groups to their hydrogen counterparts) and aromatizing (i.e. converting the cyclohexadiene units to aromatic phenyl groups) are the final steps in the synthesis of a CPP (shown in Figure 22). The alcohol (OH) groups are first deprotected using tert-butyl ammonium fluoride (TBAF), then the rings are aromatized using a reducing agent (i.e. $\mathbf{H_2SnCl_4}$) to afford the final cycloparaphenylene molecule (e.g. ***[9+1]CPP***). The deprotection involves combining the TES-containing molecule (e.g. ***[9+1]mac hexaTES***) and TBAF in a THF solution, which is then stirred at room temperature until the reaction is complete and quenched with deionized water. The aromatization involves combining the now-deprotected macrocycle (e.g. ***[9+1]mac hexol***) with a prepared

H_2SnCl_4 solution (HCl and $SnCl_2 \bullet 2H_2O$ in THF) in THF at room temperature. This mixture is then stirred under an inert atmosphere at room temperature until complete, and quenched with aqueous sodium bicarbonate.

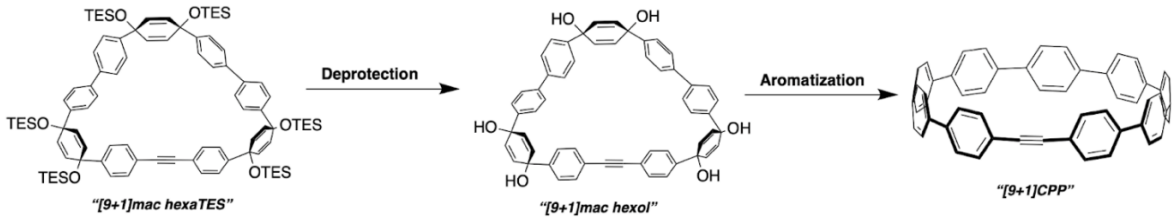

Figure 22. Reaction scheme for the deprotection and aromatization of [9+1]CPP.

Diels-Alder Reaction

This reaction culminates in the formation of two new carbon-carbon bonds using relatively mild conditions. A diene (e.g. **1,3-butadiene** or ***TPCPD***) and a dienophile (e.g. **ethylene** or ***[9+1]CPP***) are combined in a solution (e.g. **Xylenes/DMSO**), which is then heated overnight before being allowed to cool to room temperature (Figure 23).

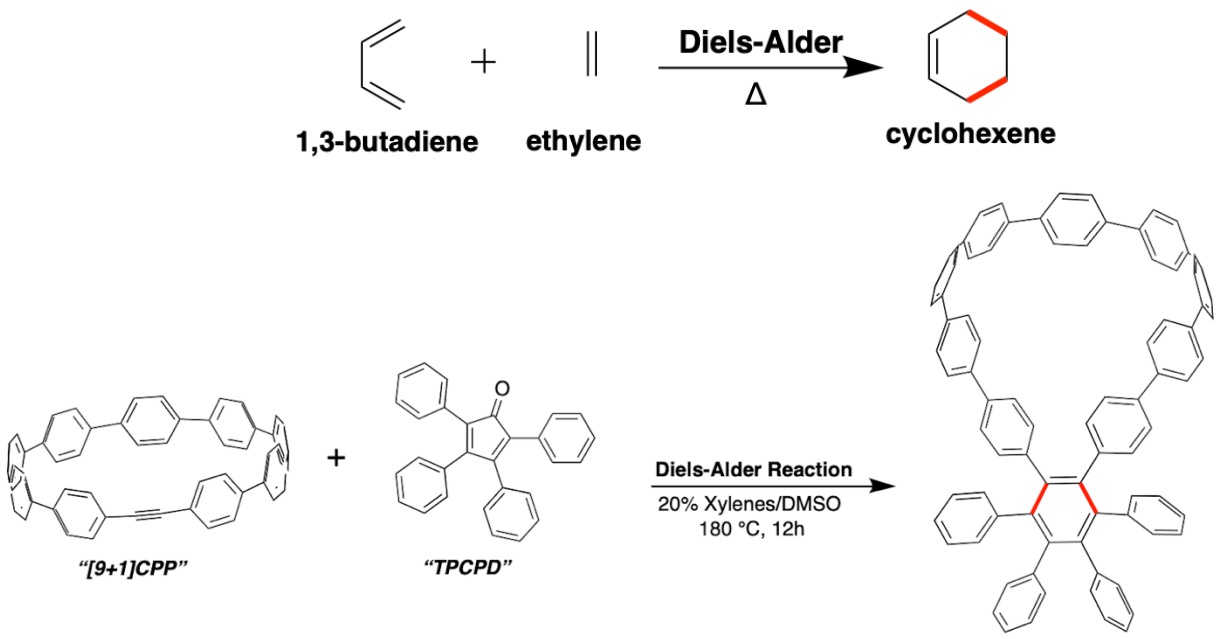

Figure 23. Scheme of a simple Diels-Alder reaction (top), and the reaction of interest in this project (bottom). Newly-formed C-C bonds shown in red.

III.III Purification Methods

Liquid Extraction

This process takes advantage of the different solubilities and densities of various organic and aqueous solvents in order to isolate the desired synthetic product from other unwanted materials (i.e. byproducts, excess unreacted starting materials). Standard liquid-liquid extraction protocols involve adding the crude reaction products to a mixture of an aqueous solution (e.g. water, brine) and an organic solvent (e.g. ethyl acetate, methylene chloride) in a separatory funnel. Since these will have different densities, two separate layers will form. Generally, the desired synthetics are organic molecules that are more miscible in the organic layer, and the aqueous layer collects any water-soluble impurities. After a few washes, the organic layer is dried with sodium sulfate, filtered, and eventually subjected to rotary evaporation, yielding the crude, distilled product.

Precipitation/Recrystallization

This process also relies on solubilities of different materials. When an impure product is dissolved in a low-solubility solvent, it will precipitate (i.e. "crash out"), which ideally yields the pure desired product in solid form while impurities remain dissolved in solution. This effect can be improved with varying temperatures, such as placing the impure product in solution in the freezer, as the solubility of the impure product in solution decreases at colder temperatures.

Flash Column Chromatography

This process relies on differences between the molecular polarities of the desired product and impurities, as this technique separates the molecules based on their polarity. The crude product is loaded onto a silica or alumina gel column and washed with a predetermined solvent mixture. This solvent is carefully chosen through a series of thin-layer chromatography (TLC) analyses, which can indicate the ideal solvent polarity (achieved by mixing a polar and non-polar solvent) to isolate the desired product from impurities as it travels through the column. Once the sample is loaded onto the column, the process is accelerated by pushing air through and small fractions are collected. With more TLC analyses, fractions can be combined and subjected to rotary evaporation, yielding the pure product.

Characterization

^{1}H (proton) NMR spectra were recorded using a Varian INOVA-500 at 500 MHz and a Bruker Avance III-HD at 600 MHz. ^{13}C (carbon) NMR spectra will be recorded using the Bruker Avance III-HD at 600 MHz. All ^{1}H NMR samples were dissolved in deuterated chloroform ($CDCl_3$).

III.IV Materials

Substrates

The molecular building blocks key to the CPP synthesis were assembled from commercially available starting materials (Figure 24).

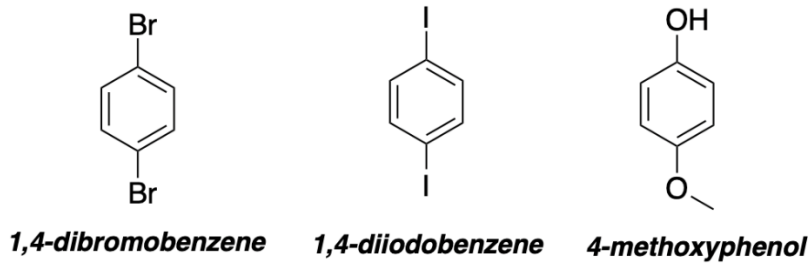

Figure 24. Commercially available materials used in this project.

Solvents

Reactions specific to the CPP synthesis were performed in one of the following solvents: tetrahydrofuran (THF), dimethyl formamide (DMF), dichloromethane (DCM), acetonitrile, and 1,4-dioxane. These solvents were stored under an inert (argon) atmosphere in a PPT dry-solvent purification system and retrieved using needles and syringes. Additional solvents stored under air were used throughout the project. The Diels-Alder reaction was performed in a Xylenes and dimethyl sulfoxide (DMSO) solution which was dried under vacuum and cycled with nitrogen gas.

Chapter IV. Supplemental Experimental Details

IV.I Synthesis of 9a

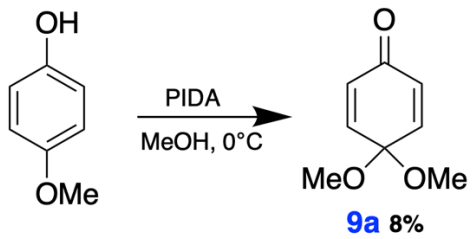

4-methoxyphenol (100 g, 805 mmol, 1 eq) was dissolved in methanol (900 mL) in a flame-dried round-bottom flask equipped with a stir bar. The mixture was cooled in a water/ice bath to 0 °C over 30 minutes. Phenyliodine diacetate (249 g, 805 mmol, 1 eq) was then added incrementally over the course of one hour, and the resulting amber/yellow reaction mixture was sealed and allowed to stir overnight under a nitrogen atmosphere. The reaction was quenched with aqueous sodium bicarbonate (500 mL) and extracted with dichloromethane (4x50 mL). The extract was dried with sodium sulfate, subjected to vacuum filtration, and the excess dichloromethane was removed via rotary evaporation. The resulting red oil was subjected to vacuum distillation for 48-72 hours at 55 °C, yielding a yellow oil which was then purified via column chromatography in a 10% ethyl acetate/hexanes solution on basic alumina. Due to time constraints, only the necessary amount of crude product was purified (10.0323 g, 8%), and the remaining crude product was stored in a freezer. ^{1}H NMR (600 MHz, Chloroform-*d*) δ 6.73 (d, *J* = 10.5 Hz, 2H), 6.16 (d, *J* = 10.4 Hz, 2H), 3.27 (s, 6H) ppm.

IV.II Synthesis of 9b

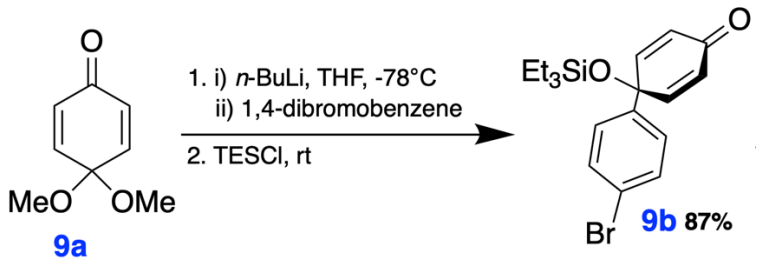

1,4-Dibromobenzene (5.5 g, 0.0204 mol, 1.2 eq) was added to a flame-dried round-bottom flask equipped with a stir bar and dissolved in THF (28 mL, 0.7 M) under a nitrogen atmosphere. The reaction was then cooled to -78 °C in an acetone/dry ice bath over the course of 30 minutes. Then, *n*-BuLi (8.17 mL, 1.05eq, 2.5 M in hexanes) was added dropwise followed a few minutes later by the addition of **9a** (2.72 mL, 0.0194 mol, 1 eq) dropwise. The reaction was then allowed to stir at -78 °C for an hour. Chlorotriethylsilane was added (3.92 mL, 0.0233 mol, 1.2 eq) and the reaction was allowed to warm to room temperature and stirred overnight. The reaction was quenched with deionized water, and the mixture was stirred for 20 minutes. The solvent was removed via rotary evaporation, and the mixture was then extracted with ethyl acetate (3x100 mL), washed with brine (3x100mL), dried over sodium sulfate, gravity filtered, and concentrated to yield the crude product as an amber oil. The crude product was then purified via column chromatography in a 5% EtOAc/hexanes solution on silica (6.4411 g, 19 mmol, 87%). ^{1}H NMR (600 MHz, Chloroform-*d*) δ 6.73 (d, *J* = 10.5 Hz, 2H), 6.16 (d, *J* = 10.4 Hz, 2H), 3.27 (s, 6H) ppm.

IV.III Synthesis of 9c

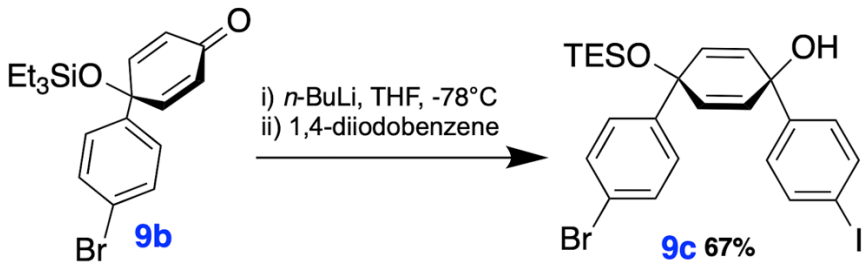

1,4-Diiodobenzene (7.00 g, 21.11 mmol, 1.25 eq) was dissolved in THF (78 mL, 0.219 M,) and the solution was cooled to -78 °C. n-BuLi (2.5 M in hexanes, 8.2 mL, 1.2 eq) was added dropwise over 5 minutes. After stirring the reaction mixture for a few minutes, **9b** (6.44 g, 16.97 mmol, 1 eq) dissolved in THF (16 mL, 1.09 M) was added dropwise via syringe at -78 °C. The resulting reaction mixture was stirred for 1 hour at -78 °C, then quenched by addition of water (20 mL) and the reaction mixture was allowed to warm to room temperature. EtOAc (70 mL) was added and the aqueous phase was extracted with EtOAc (3x50 mL). The combined organic phases were washed with brine (2x40 mL), dried over sodium sulfate, and the solvent was removed with a rotary evaporator. The crude product was purified by column chromatography on silica in a 5% EtOAc/hexanes solution, yielding a highly viscous yellow oil (6.6157 g, 11 mmol, 67%). ^{1}H NMR (600 MHz, Chloroform-d) δ 7.69 (d, J = 8.5 Hz, 2H), 7.42 (d, J = 8.6 Hz, 2H), 7.22 (d, J = 8.6 Hz, 2H), 7.18 (d, J = 8.6 Hz, 4H), 2.02 (s, 1H), 0.99 (t, J = 7.9 Hz, 9H), 0.68 (q, J = 7.9 Hz, 6H) ppm.

IV.IV Synthesis of 9d

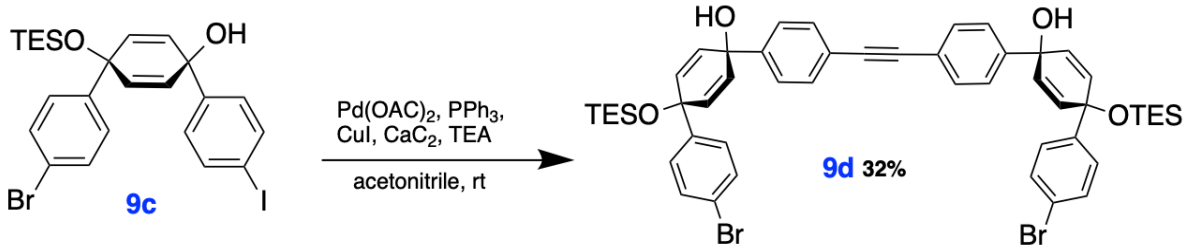

A solution of palladium acetate (10 mg, 0.04 mmol, 0.02 eq), triphenylphosphine (29 mg, 0.11 mmol, 0.05 eq), and copper iodide (21 mg, 0.11 mmol, 0.05 eq) in wet acetonitrile (6 mL, 0.2 M) was sparged with nitrogen gas for 1 hour in a flame-dried flask equipped with a stir bar. **9c** (1.3 g, 2.22 mmol, 1 eq) in wet acetonitrile (6 mL, 0.2 M) in a separate flame-dried flask was also sparged with nitrogen gas for 1 hour. Then, triethylamine (10 mL, 6.66 mmol, 3 eq), calcium carbide (0.4269 g, 6.66 mmol, 3 eq), and **9c** (1.2952 g, 2.22 mmol, 1 eq) were added to the flask containing the catalysts. The light brown reaction mixture was stirred at room temperature under nitrogen atmosphere for 24-72 hours. Then, the mixture was filtered through a short plug of Celite to remove solids, and the solvent was removed under reduced pressure. The crude product was purified by column chromatography on silica in 0-100% DCM/hexanes, yielding the product as a yellow oil (tan foam under high vacuum) (0.6684 g, 2.22 mmol, 32%). ^{1}H NMR (600 MHz, Chloroform-*d*) δ 7.52 (d, *J* = 8.6 Hz, 4H), 7.42 (dd, *J* = 8.5, 1.8 Hz, 8H), 7.24 (d, *J* = 3.9 Hz, 4H), 5.99 (dd, 8H), 2.06 (s, 2H), 1.00 (t, 18H), 0.69 (q, *J* = 7.9, 3.5 Hz, 12H) ppm.

IV.V Synthesis of 9e

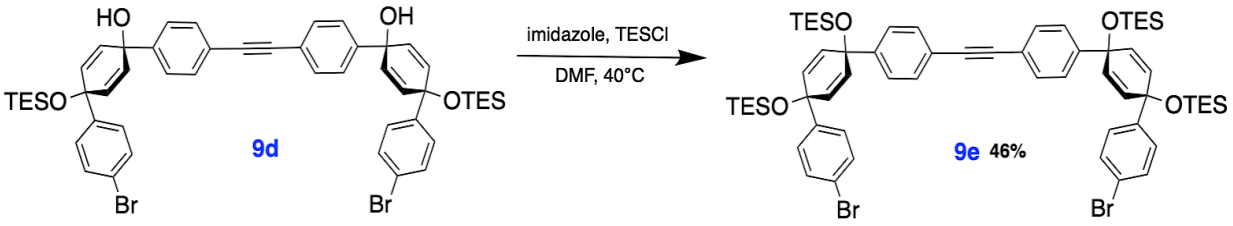

9d (0.5846 g, 0.62 mmol, 1 eq) and imidazole (0.127 g, 1.87 mmol, 3 eq) were dissolved in dry DMF (5 mL). Chlorotriethylsilane (0.23 mL, 1.37 mmol, 2.2 eq) was added and the reaction was sparged with nitrogen gas for 20 minutes, then stirred at 40 °C overnight. The reaction was quenched with aqueous sodium bicarbonate and extracted with DCM (2x20 mL). The combined organic layers were washed with brine and dried over sodium sulfate. The solvent was removed to yield a yellow oil, which under high vacuum resulted in a yellow solid. This was purified by column chromatography on silica in 0-10% DCM/hexanes, yielding the product as a colorless, highly viscous oil that was stored in the freezer, eventually precipitating as a white powder (0.331 g, 0.28 mmol, 46%). ^{1}H NMR (600 MHz, Chloroform-*d*) δ 7.46 (d, *J* = 8.4 Hz, 4H), 7.40 (d, *J* = 8.6 Hz, 4H), 7.31 (d, *J* = 8.4 Hz, 4H), 7.20 (d, *J* = 8.6 Hz, 4H), 5.99 (q, 8H), 0.95 (q, 36H), 0.68 – 0.49 (m, 24H) ppm.

IV.VI Synthesis of 9g

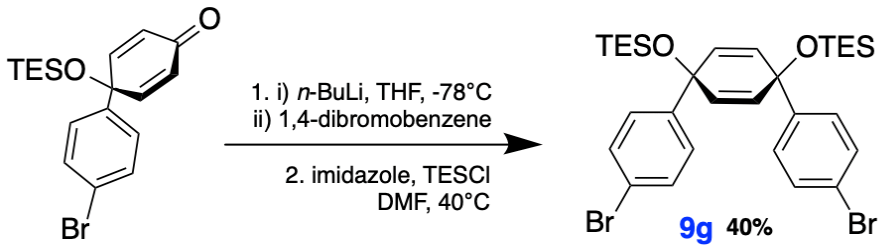

1,4-Dibromobenzene (306.7 mg, 1.3 mmol, 1.25 eq) was dissolved in dry THF (5 mL, 0.219 M) and the solution was cooled to -78 °C in an acetone/dry ice bath for 30 minutes. *n*-

BuLi (0.5 mL, 1.2 eq, 2.5 M in hexanes) was added dropwise. **9b** was dissolved in dichloromethane, transferred to a separate reaction flask, and the solvent was removed via rotary evaporation before the flask was dried under vacuum/N_2 gas. **9b** (0.3946 g, 10.4 mmol, 1 eq) was dissolved in THF (2 mL, 1.09 M) and cooled to -78 °C in an acetone/dry ice bath. After 10 minutes, **9b** was added dropwise via syringe at -78 °C to the flask containing the 1,4-dibromobenzene. The resulting reaction mixture was stirred for 1 hour at -78 °C, before being quenched by the addition of deionized water (20 mL) and allowed to warm to room temperature. EtOAc (70 mL) was added, and the aqueous phase was further extracted with EtOAc (3x50 mL). The combined organic phases were washed with brine (2x50 mL), dried over sodium sulfate, and the solvent was removed via rotary evaporation. The total crude product (0.456 g, 0.85 mmol, 1 eq) was then directly combined with imidazole (0.23 g, 3.40 mmol, 1 eq) in another flame-dried flask equipped with a stir bar, and dissolved in dry DMF (5 mL, 0.2 M) at room temperature. Chlorotriethylsilane (0.21 mL, 1.27 mmol, 1.5 eq) was added dropwise to the solution, and the flask was immersed in an oil bath that was pre-heated to 40 °C and stirred overnight. The reaction mixture was allowed to cool to room temperature before being quenched with saturated aqueous sodium bicarbonate. The aqueous phase was extracted with ethyl acetate (3x30 mL), and the organic layers were washed with bring (2x20 mL), aqueous LiCl solution (2x20 mL), and dried with sodium sulfate. The solvent was removed via rotary evaporation, yielding the crude product as an amber oil that was purified via column chromatography in 100% hexanes on silica, affording the pure product as a faint yellow oil (0.2197 g, 0.337 mmol, 40%). ^{1}H NMR (600 MHz, Chloroform-*d*) δ 7.31 (d, J = 8.6 Hz, 4H), 7.22 (d, J = 8.6 Hz, 4H), 5.98 (s, 4H), 0.99 (t, J = 7.9 Hz, 18H), 0.68 (q, J = 7.9 Hz, 12H) ppm.

IV.VII Synthesis of 9f

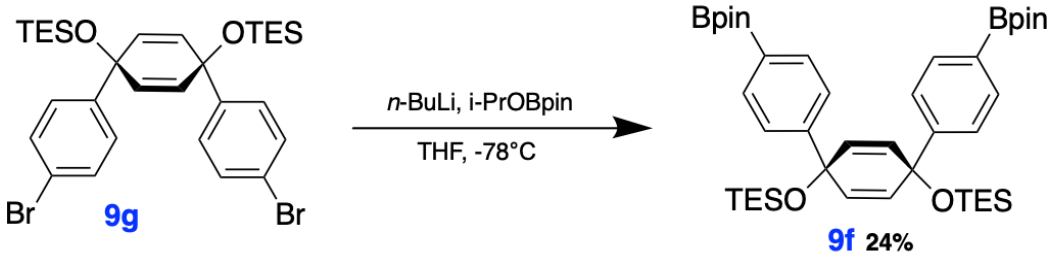

A solution of **9g** (0.2197 g, 0.33 mmol, 1 eq.) in THF (1.6 mL, 0.2 M) was cooled to –78 °C over 30 minutes. *n*-BuLi (2.5 M in hexanes, 0.31 mL, 0.77 mmol, 2.3 eq.) was added dropwise at –78 °C. After the addition the reaction mixture was stirred at –78 °C for 5 minutes before 2-isopropoxy- 4,4,5,5-tetramethyl-1,3,2-dioxaborolane "i-PrOBpin" (0.21 mL, 1.01 mmol, 3 eq.) was added dropwise. For 1 hour, the reaction was allowed to warm to room temperature while the ice bath was not replenished. After 1 hour, the reaction mixture was removed from the ice bath and allowed to completely warm to room temperature, then quenched with water. The mixture was extracted with EtOAc (3x100 mL). The combined organic phases were washed with water (2x100 mL) and brine (100 mL), dried over sodium sulfate, and the solvent was removed under reduced pressure, and the residue was placed under high vacuum to yield a viscous yellow oil. Sonication in methanol for approximately 10 minutes, yielded a white solid, which was isolated via vacuum filtration (0.0596 g, 24%). ^{1}H NMR (600 MHz, Chloroform-d) δ 7.70 (d, J = 7.7 Hz, 4H), 7.34 (d, J = 7.7 Hz, 4H), 5.96 (s, 4H), 1.34 (s, 24H), 0.92 (t, J = 8.0 Hz, 18H), 0.59 (q, J = 7.9 Hz, 12H) ppm.

IV.VIII Synthesis of 9h

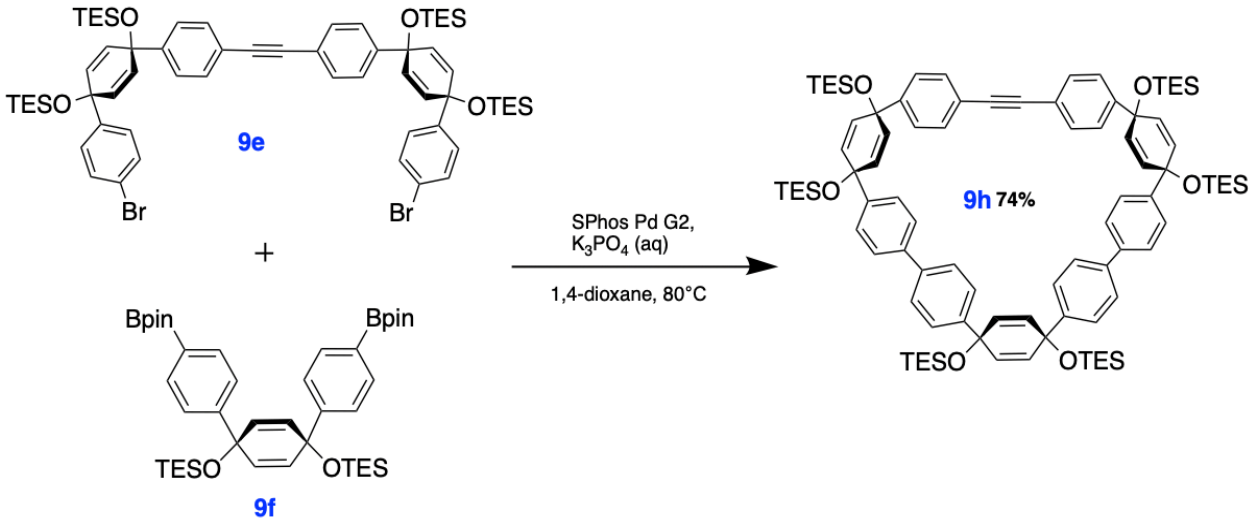

9e (0.0847 g, 0.07 mmol, 1.00 eq), **9f** (0.0596 g, 0.08 mmol, 1.1 eq), and Chloro(2-dicyclohexylphosphino-2',6'-dimethoxy-1,1'-biphenyl)[2-(2'-amino-1,1'-biphenyl)]palladium(II) (SPhos Pd G2, 5.24 mg, 0.007 mmol, 0.1 eq) were added to a flame-dried flask equipped with a stir bar, and the flask was evacuated/backfilled with nitrogen five times. Then, deoxygenated 1,4-dioxane (32 mL, 0.00225 M) was added and the resulting solution was stirred and sparged with nitrogen gas for 30 minutes at room temperature while an oil bath was preheated 80 °C. After 30 minutes, sparging was halted and the reaction mixture was placed in the oil bath and allowed to stir for another 30 minutes. Then, deoxygenated aqueous K_3PO_4 solution (0.0225 M, 3.2 mL) was added via syringe. The reaction was stirred at 80 °C overnight, under a nitrogen atmosphere. The next day, the reaction mixture (now brown in color) was removed from heat and allowed to cool to room temperature for approximately 20 minutes, then filtered through a Celite plug topped with sodium sulfate and washed through with DCM. The filtrate was further dried over sodium sulfate, filtered, and concentrated to yield the crude product as a yellow oil (blue/teal under UV light) that was then purified using column chromatography on silica in 0-5% EtOAc/hexanes, yielding a yellow oil (0.081 g, 74%). ^{1}H NMR (600 MHz, Chloroform-*d*) δ 7.58

(d, J = 8.5 Hz, 4H), 7.53 (d, J = 8.2 Hz, 4H), 7.49 (d, J = 7.9 Hz, 4H), 7.44 (d, J = 8.5 Hz, 4H), 7.34 (d, J = 8.6 Hz, 4H), 7.32 (d, 4H), 6.01 (s, 12H), 1.00 – 0.82 (m, 54H), 0.69 – 0.59 (m, 36H) ppm.

IV.IX Synthesis of 9i

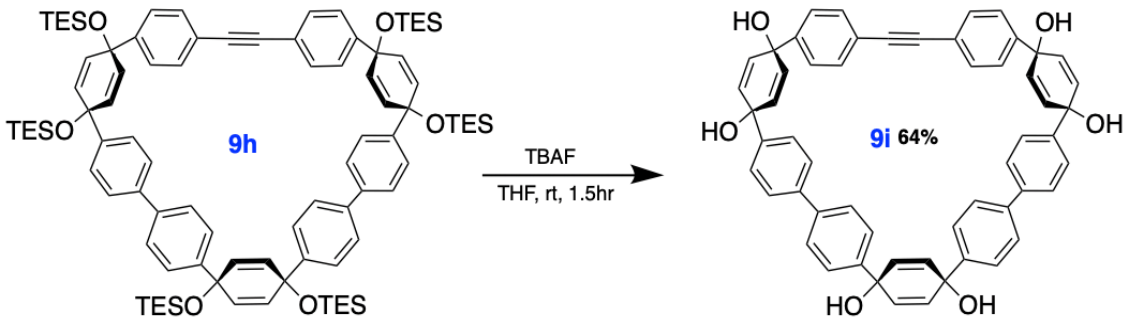

9h (0.106g, 0.05mmol, 1eq) was dissolved in THF (6.8 mL, 0.02 M), and tetrabutylammonium fluoride (1 M, 0.36 mL, 0.35 mmol, 6.6 eq) was added at room temperature, turning the yellow mixture to amber/orange. The reaction mixture stirred for 1.5 hours before being transferred to a larger flask and quenched with water (40 mL), and the THF was removed under reduced pressure. The resulting solid was filtered off and thoroughly washed with water and DCM to afford the product as a yellow solid (0.0367 g, 0.0452 mmol, 64%) that was directly subjected to aromatization due to its insolubility in available NMR solvents.

IV.X Synthesis of 9j

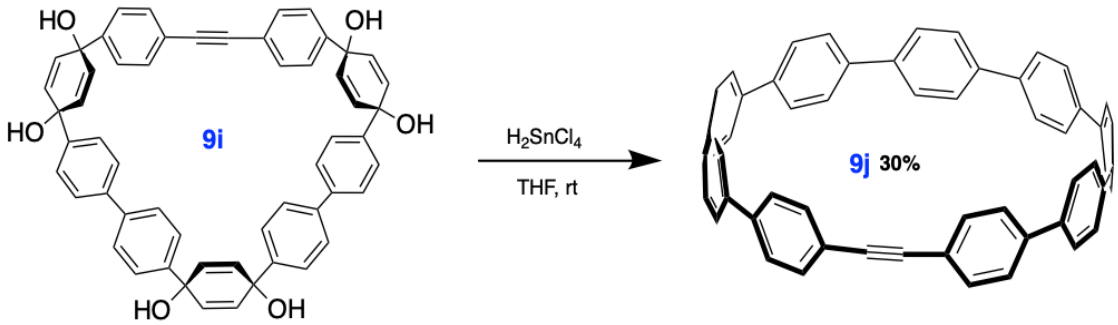

A solution of H_2SnCl_4 was prepared beforehand in a flame-dried flask by adding concentrated aqueous HCl (0.33 mL, 0.07 mmol, 12 M, 2 eq) to $SnCl_2•2H_2O$ (0.4513 g, 0.036 mmol, 1 eq) and dissolving in THF (50 mL, 0.04 M). This solution was allowed to stir under nitrogen atmosphere for 30 mins at room temperature. **9i**, which had been stored in two fractions (#1, 1.9 mL, 0.075 mmol, 0.04 M, 1 eq) (#2, 1.1 mL, 0.043 mL, 0.04 M, 1 eq), was dissolved in dry THF and stirred under a nitrogen atmosphere. Then, the H_2SnCl_4 solution was added (#1, 1.9 mL, 0.075 mmol, 0.04 M, 1eq) (#2, 1.1 mL, 0.043 mL, 0.04 M, 1 eq) and the orange mixtures were stirred under nitrogen atmosphere for 1 hour. Then, each reaction mixture was quenched with an aqueous solution of sodium bicarbonate. TLC on alumina in 50% DCM/hexanes indicated both fractions could be combined. The combined solution was extracted with DCM, washed with brine, dried with sodium sulfate, and concentrated to afford a yellow solid (blue fluorescence). An alumina plug in 50% DCM/hexanes was run on the crude product, yielding a blue-fluorescent filtrate that was concentrated to yield a yellow solid (0.0076 g, 0.0107 mmol, 30%). ^{1}H NMR (600 MHz, Chloroform-d) δ 7.61 – 7.51 (m, 28H), 7.49 (d, J = 5.8 Hz, 4H), 7.37 (d, J = 8.3 Hz, 4H) ppm.

IV.XI Synthesis of 9k

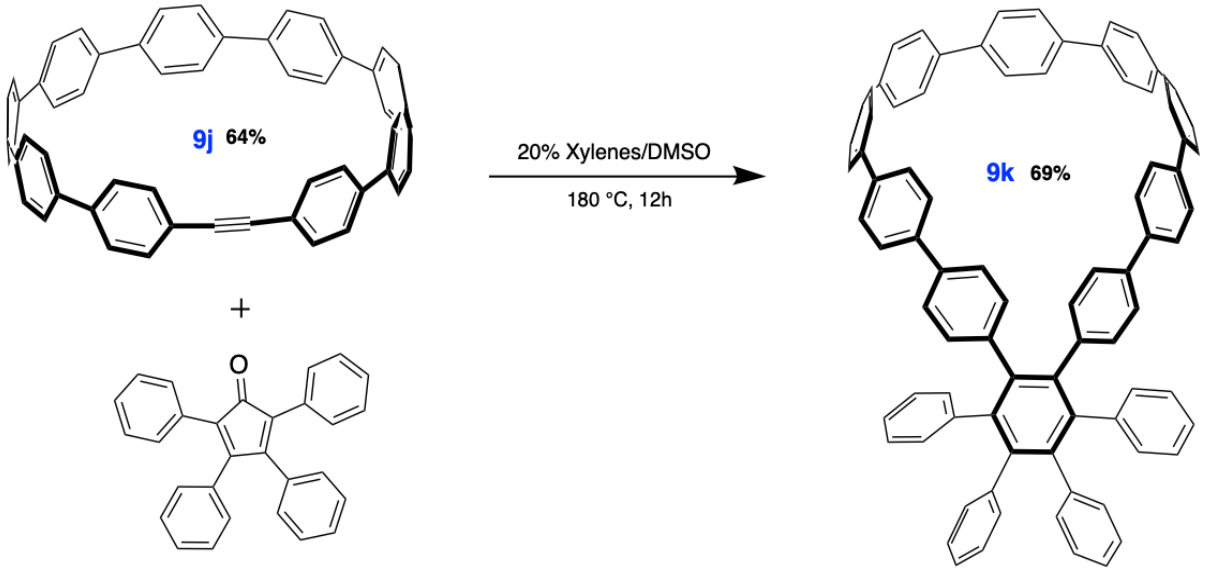

9j (7.6 mg, 0.0107 mmol, 1 eq) in a scintillation vial was dried under high vacuum and cycled under nitrogen atmosphere, then dissolved in a mixture of 20% Xylene/DMSO (1.07 mL total, 0.01 M, 0.24 mL xylene, 0.86 mL DMSO) added via syringe. The mixture was then transferred via syringe to a microwave vial, and heated to 180 °C for 12 hours, yielding a dark red crude product (teal fluorescence under UV light). The DMSO was removed via rotary evaporation, and the crude product was subjected to an alumina plug in 0-25% DCM/hexanes, yielding a red oil. The crude reaction mixture (red) was then diluted in minimal hexanes, forming a yellow (green fluorescent) precipitate. The reaction flask was then rinsed with hexanes, and the precipitate was dissolved in DCM. TLC in 50% DCM/hexanes indicated that the yellow precipitate is likely the product. The pure product was concentrated and dried under vacuum for >24 hours, then sonicated in pentanes, allowed to settle, and the solvent was removed via pipette. The precipitate was dissolved in minimal DCM and concentrated, yielding a yellow solid (green fluorescence) (7.9 mg, 0.00741 mmol, 69%). ^{1}H NMR (600 MHz, Chloroform-*d*) δ 7.46 (s, 4H), 7.40 (q, *J* = 8.9 Hz, 10H), 7.31 (dd, *J* = 6.3, 2.0 Hz, 14H), 7.00 (d, *J* = 8.2 Hz, 4H), 6.78 – 6.69 (m, 24H) ppm.

References

1. White, Brittany M., Yu Zhao, Taryn E. Kawashima, Bruce P. Branchaud, Michael D. Pluth, and Ramesh Jasti. "Expanding the Chemical Space of Biocompatible Fluorophores: Nanohoops in Cells." *ACS Central Science* 4, no. 9 (September 26, 2018): 1173–78. https://doi.org/10.1021/acscentsci.8b00346.

2. Fluorescence Fundamentals | Thermo Fisher Scientific - US https://www.thermofisher.com/us/en/home/references/molecular-probes-thehandbook/introduction-to-fluorescence-techniques.html (accessed May 20 2023).

3. Lavis, Luke D., and Ronald T. Raines. "Bright Ideas for Chemical Biology." *ACS Chemical Biology* 3, no. 3 (March 1, 2008): 142–55. https://doi.org/10.1021/cb700248m.

4. Boyd V, Cholewa OM, Papas KK. Limitations in the Use of Fluorescein Diacetate/Propidium Iodide (FDA/PI) and Cell Permeable Nucleic Acid Stains for Viability Measurements of Isolated Islets of Langerhans. *Curr Trends Biotechnol Pharm*. 2008 Mar;2(2):66-84.

5. Valdes-Aguilera, O., Cincotta, L., Foley, J. and Kochevar, I.E. (1987), Photobleaching of a Cyanine Dye in Solution and in Membranes. *Photochemistry and Photobiology*, 45: 337-344. https://doi.org/10.1111/j.1751-1097.1987.tb05384.x

6. Hirst, Elizabeth S., and Ramesh Jasti. "Bending Benzene: Syntheses of [*n*]Cycloparaphenylenes." *The Journal of Organic Chemistry* 77, no. 23 (December 7, 2012): 10473–78. https://doi.org/10.1021/jo302186h.

7. Jasti, Ramesh, Joydeep Bhattacharjee, Jeffrey B. Neaton, and Carolyn R. Bertozzi. "Synthesis, Characterization, and Theory of [9]-, [12]-, and [18]Cycloparaphenylene: Carbon Nanohoop Structures." *Journal of the American Chemical Society* 130, no. 52 (December 31, 2008): 17646–47. https://doi.org/10.1021/ja807126u.

8. Iwamoto, Takahiro, Yoshiki Watanabe, Youichi Sakamoto, Toshiyasu Suzuki, and Shigeru Yamago. "Selective and Random Syntheses of [*n*]Cycloparaphenylenes (*n* = 8–13) and Size Dependence of Their Electronic Properties." *Journal of the American Chemical Society* 133, no. 21 (June 1, 2011): 8354–61. https://doi.org/10.1021/ja2020668.

9. Segawa, Y.; Fukazawa, A.; Matsuura, S.; Omachi, H.; Yamaguchi, S.; Irle, S.; Itami, K. Combined Experimental and Theoretical Studies on the Photophysical Properties of Cycloparaphenylenes. *Organic & Biomolecular Chemistry* 2012, *10* (30), 5979. https://doi.org/10.1039/c2ob25199j.

10. Wong, Bryan M. “Optoelectronic Properties of Carbon Nanorings: Excitonic Effects from Time-Dependent Density Functional Theory.” *The Journal of Physical Chemistry C* 113, no. 52 (December 31, 2009): 21921–27. https://doi.org/10.1021/jp9074674.

11. Darzi, E. R.; Jasti, R. The Dynamic, Size-Dependent Properties of [5]–[12]Cycloparaphenylenes. *Chemical Society Reviews* 2015, *44* (18), 6401–6410. https://doi.org/10.1039/C5CS00143A.

12. Lefebvre, J.; Ding, J.; Li, Z.; Finnie, P.; Lopinski, G.; Malenfant, P. R. L. High-Purity Semiconducting Single-Walled Carbon Nanotubes: A Key Enabling Material in Emerging Electronics. *Acc. Chem. Res.* 2017, 50 (10), 2479–2486. 10.1021/acs.accounts.7b00234

13. Leonhardt, E. J.; Jasti, R. Emerging Applications of Carbon Nanohoops. *Nat. Rev. Chem.* 2019, 3, 672-686. https://doi.org/10.1002/anie.201901984

14. Maust, R.; Li, P.; Zakharov, L. N.; Jasti, R. Cycloparaphenylene-Norbornene Monomers Afford Access to Carbon Nanohoop-Based Polymers. *ChemRxiv* 2019, 1–28.

15. Van Raden, J. M.; Darzi, E. R.; Zakharov, L. N.; Jasti, R. Synthesis and Characterization of a Highly Strained Donor-Acceptor Nanohoop. *Org. Biomol. Chem.* 2016, 14 (24), 5721–5727.

16. White, Brittany M., Yu Zhao, Taryn E. Kawashima, Bruce P. Branchaud, Michael D. Pluth, and Ramesh Jasti. “Expanding the Chemical Space of Biocompatible Fluorophores: Nanohoops in Cells.” *ACS Central Science* 4, no. 9 (September 26, 2018): 1173–78. https://doi.org/10.1021/acscentsci.8b00346.

17. Lleres, D.; Swift, S.; Lamond, A.; Detecting Protein-Protein Interactions In Vivo with FRET using Multiphoton Fluorescence Lifetime Imaging Microscopy (FLIM) *Curr. Protocol. Cytom.* 2007, 1934-9300. doi:10.1002/0471142956.cy1210s42

18. Van Raden, Jeff M., Brittany M. White, Lev N. Zakharov, and Ramesh Jasti. “Nanohoop Rotaxanes from Active Metal Template Syntheses and Their Potential in Sensing Applications.” *Angewandte Chemie International Edition* 58, no. 22 (May 27, 2019): 7341–45. https://doi.org/10.1002/anie.201901984.

19. Leonhardt, E. J.; Jasti, R. Emerging Applications of Carbon Nanohoops. *Nat. Rev. Chem.* 2019, 3, 672-686. https://doi.org/10.1002/anie.201901984

20. Parekh, V. C.; Guha, P. C. Synthesis of pp'-Diphenylenedimonosulphide. *J. Indian Chem. Soc.* 1934, *11*, 95.

21. Schaub, Tobias A., Johannes T. Margraf, Lev Zakharov, Karsten Reuter, and Ramesh Jasti. “Strain-Promoted Reactivity of Alkyne-Containing Cycloparaphenylenes.” *Angewandte Chemie International Edition* 57, no. 50 (December 10, 2018): 16348–53. https://doi.org/10.1002/anie.201808611.

22. Devaraj, Neal K., and M. G. Finn. “Introduction: Click Chemistry.” *Chemical Reviews* 121, no. 12 (June 23, 2021): 6697–98. https://doi.org/10.1021/acs.chemrev.1c00469.

23. Garrison, Anna. “Cycloparaphenylenes and Their Biological Applications.” CHC Thesis, n.d.

24. Kolb, Hartmuth C., M. G. Finn, and K. Barry Sharpless. “Click Chemistry: Diverse Chemical Function from a Few Good Reactions.” *Angewandte Chemie International Edition* 40, no. 11 (June 1, 2001): 2004–21. https://doi.org/10.1002/1521-3773(20010601)40:11<2004::AID-ANIE2004>3.0.CO;2-5.

25. Laird, Darin W., and John C. Gilbert. “Norbornyne: A Cycloalkyne Reacting Like A Dicarbene.” *Journal of the American Chemical Society* 123, no. 27 (July 1, 2001): 6704–5. https://doi.org/10.1021/ja010589h.

26. Medina, Jose M., Travis C. McMahon, Gonzalo Jiménez-Osés, K. N. Houk, and Neil K. Garg. “Cycloadditions of Cyclohexynes and Cyclopentyne.” *Journal of the American Chemical Society* 136, no. 42 (October 22, 2014): 14706–9. https://doi.org/10.1021/ja508635v.

27. *Click Chemistry Reactions: CuAAC, SPAAC, Diels-Alder | Biopharma PEG.* www.biochempeg.com. https://www.biochempeg.com/article/71.html (accessed 2023-06-01).

28. Sigma Aldrich. Diels–Alder Reaction. *Organic Reaction Toolbox* n.d.

29. Houk, Kendall N., Fang Liu, Zhongyue Yang, and Jeffrey I. Seeman. “Evolution of the Diels–Alder Reaction Mechanism since the 1930s: Woodward, Houk with Woodward, and the Influence of Computational Chemistry on Understanding Cycloadditions.” *Angewandte Chemie International Edition* 60, no. 23 (June 2021): 12660–81. https://doi.org/10.1002/anie.202001654.

30. Gregoritza, M.; Brandl, F. P. The Diels–Alder Reaction: A Powerful Tool for the Design of Drug Delivery Systems and Biomaterials. *European Journal of Pharmaceutics and Biopharmaceutics* 2015, *97* (0939-6411), 438–453. https://doi.org/10.1016/j.ejpb.2015.06.007

31. Funel, J.-A.; Abele, S. Industrial Applications of the Diels-Alder Reaction. *Ange. Chem. Int. Ed.* 2013, *52* (14), 3822–3863. https://doi.org/10.1002/anie.201201636

32. CAS DataBase List. Tetraphenylcyclopentadienone, https://www.chemicalbook.com/ChemicalProductProperty_EN_CB8761453.htm#:~:text=and%20organometallic%20compounds.-,Uses,active%20pharmaceuticals%20and%20food%20ingredients (accessed May 10 2023)

33. Anna Chiara Sale; Murray, A. H.; Dominik Prenzel; Hampel, F.; Lidia De Luca; Tykwinski, R. R. Diels-Alder Cycloaddition of Tetraphenylcyclopentadienone and 1,3,5-Hexatriynes. *European Journal of Organic Chemistry*, 2016, *2016* (13), 2274–2283. https://doi.org/10.1002/ejoc.201600116

34. Krompiec, Stanisław, Aneta Kurpanik-Wójcik, Marek Matussek, Bogumiła Gołek, Angelika Mieszczanin, and Aleksandra Fijołek. "Diels–Alder Cycloaddition with CO, CO2, SO2, or N2 Extrusion: A Powerful Tool for Material Chemistry." *Materials* 15, no. 1 (December 27, 2021): 172. https://doi.org/10.3390/ma15010172.